Published in final edited form as:
Math Biosci. 2013 January ; 241(1): 56–74. doi:10.1016/j.mbs.2012.09.003.

Patient-specific modeling of cardiovascular and respiratory dynamics during hypercapnia

L.M. Ellwein[a], **S.R. Pope**[b], **A. Xie**[c], **J.J. Batzel**[d], **C.T. Kelley**[e], and **M.S. Olufsen**[e]

[a]Dept. of Mathematics, Virginia Commonwealth University, Richmond, VA, USA

[b]*SAS, Cary, NC, USA*

[c]Pulmonary Physiology Laboratory, William S. Middleton Veterans Hospital, Madison, WI, USA

[d]Inst. for Math. and Scientific Computing, Univ. of Graz, Graz, Austria

[e]Dept. of Mathematics, North Carolina State University, Raleigh, NC, USA

Abstract

This study develops a lumped cardiovascular-respiratory system-level model that incorporates patient-specific data to predict cardiorespiratory response to hyper-capnia (increased CO_2 partial pressure) for a patient with congestive heart failure (CHF). In particular, the study focuses on predicting cerebral CO_2 reactivity, which can be defined as the ability of vessels in the cerebral vasculature to expand or contract in response CO_2 induced challenges. It is difficult to characterize cerebral CO_2 reactivity directly from measurements, since no methods exist to dynamically measure vasomotion of vessels in the cerebral vasculature. In this study we show how mathematical modeling can be combined with available data to predict cerebral CO_2 reactivity via dynamic predictions of cerebral vascular resistance, which can be directly related to vasomotion of vessels in the cerebral vasculature. To this end we have developed a coupled cardiovascular and respiratory model that predicts blood pressure, flow, and concentration of gasses (CO_2 and O_2) in the systemic, cerebral, and pulmonary arteries and veins. Cerebral vascular resistance is incorporated via a model parameter separating cerebral arteries and veins. The model was adapted to a specific patient using parameter estimation combined with sensitivity analysis and subset selection. These techniques allowed estimation of cerebral vascular resistance along with other cardiovascular and respiratory parameters. Parameter estimation was carried out during eucapnia (breathing room air), first for the cardiovascular model and then for the respiratory model. Then, hypercapnia was introduced by increasing inspired CO_2 partial pressure. During eucapnia, 7 cardiovascular parameters and 4 respiratory parameters was be identified and estimated, including cerebral and systemic resistance. During the transition from eucapnia to hypercapnia, the model predicted a drop in cerebral vascular resistance consistent with cerebral vasodilation.

Keywords

sensitivity analysis; parameter estimation; physiological models; cerebral blood flow; complex models

1. Introduction

Regulation of breathing and cardiovascular dynamics as well as their interactions are essential for healthy physiological responses to CO_2 challenges. It has been shown that certain mechanisms within the cardio-respiratory regulatory system are compromised in patients suffering from congestive heart failure (CHF) and sleep apnea [1, 2, 3, 4, 5, 6], in particular, it is believed that cerebral CO_2 reactivity is muted in these patients. Moreover, a compromised cerebral CO_2 reactivity may affect the stability of breathing causing ventilatory overshooting during hypercapnia and undershooting during hypocapnia (decreased CO_2 partial pressure) [5, 6]. In the clinic, cerebral CO_2 reactivity is studied by challenging the respiratory system, e.g., by inducing hyper- or hypocapnia. The response to hypercapnia is cerebral vasodilation yielding an increase in cerebral blood flow velocity, while hypocapnia elicits opposite effects. Non-invasive measurements used to assess cerebral CO_2 reactivity include inspired volumetric airflow, expiratory CO_2 partial pressure, heart rate, ejection fraction, arterial blood pressure, and cerebral blood flow velocity. These quantities can be measured dynamically at a high temporal resolution, but they have to be interpreted to assess cerebral vasomotion. One way to combine the available measurements for prediction of cerebral vasomotion is using mathematical modeling.

Several recent studies have provided insight into the mechanisms that govern respiratory function, respiratory system interaction with cardiovascular control, and mutual regulation between ventilation and cerebral blood flow (CBF) and arterial CO_2 partial pressure. Mathematical models that address aspects of the above topics include work by Dong and Langford [7], who developed a model to study factors affecting stable behavior of the cardiovascular-respiratory system in CHF and Lu et al. [8, 9] who applied a combined cardiovascular-respiratory model to study the Valsalva maneuver and factors affecting cerebral blood flow. Relevant experimental studies include work investigating the differential role of CO_2 partial pressures and sympathetic response on vasoconstriction [10], and the role of cerebral reactivity to CO_2 [6]. In addition to understanding basic mechanisms associated with ”healthy” cardio-respiratory interactions, many studies focus on investigating mechanisms associated with pathological cardio-respiratory dynamics. Among the most studied group of patients are those suffering from CHF and sleep apnea (about half the patients with CHF have episodes of sleep apnea).

For CHF patients, an influence of cerebral reactivity on respiratory function could develop as follows. CHF patients can have an elevated brain tissue CO_2 partial pressure after being subjected to a hypercapnic challenge, with this elevation possibly resulting from a muted cerebral CO_2 reactivity. Elevated brain tissue CO_2 resulting from muted or impaired cerebral reactivity can lead to increased respiratory chemosensor stimulation and artificially raised ventilatory drive. Such changes which influence respiratory control responses may contribute to unstable breathing patterns when normal breathing is disturbed by events such as apnea-related asphyxia often observed in CHF patients [11] (arousal-related hyperpnia can have analogous effects). More detailed knowledge of cerebral vascular reactivity and related mechanisms can potentially be obtained with mathematical models that couple ventilatory and cardiovascular system dynamics and control functions combined with appropriate parameter estimation techniques.

To provide adequate physiological insights and allow prediction of specific quantities, the model must include a fair degree of complexity, yet to be able to use the model for analysis of given data, the model should be able to provide reliable model predictions. One way to render a model patient-specific is to use nonlinear optimization to predict a set of model parameters and initial conditions that minimize the least squares error between computed states and the patient-specific data. This process involves solving an inverse problem: predicting the model parameters given the model and the model output. Inverse problems are typically ill-posed and thus difficult to solve reliably. Generally, as the number of measured system quantities increases, the inverse problem becomes easier to solve, yet to minimize patient discomfort and risks, experiments are often limited to a few non-invasive quantities. At the same time, the mathematical models developed to study the system dynamics have to be fairly complex to capture necessary details of the system. Consequently, a relatively large set of parameters are associated with models where only limited data are available. Thus, it may only be possible to estimate a small subset of model parameters. Two techniques are typically employed to identify a small subset of parameters: sensitivity analysis, which predicts how sensitive the model output is to changes in parameter values, and parameter identification or subset selection, which predicts potential correlations among model parameters. If a set of parameters are correlated, only one or a given combination of the parameters can be estimated uniquely.

This study describes a comprehensive method for estimating parameters in a complex physiological model predicting the cardiovascular-respiratory response to hypercapnia in a patient with CHF. To do so, we developed a coupled cardiovascular and respiratory systems model that predicts pulsatile blood pressure, flow, and concentration of gasses (CO_2 and O_2) in the systemic, cerebral, and pulmonary arteries and veins for the patient studied. The model was applied to two respiratory conditions. First, we analyzed dynamics during 5 min of eucapnic breathing, followed by analysis of the transition to hypercapnic breathing. For each experimental condition, parameter sensitivity analysis was used to rank model parameters from the most to the least sensitive, and parameter identification was used to predict a subset of parameters that could be estimated given available data. Section 2 describes efforts needed to develop the cardiovascular (section 2.1) and respiratory (section 2.2) models as well as efforts needed to predict nominal parameters used for these models (section 2.3). Section 3 describes data used for this study, and section 4 describes efforts involved with parameter estimation. Section 5 presents our results during eucapnia (section 5.1) and hypercapnia (section 5.2), section 6 discusses our results, and section 7 summarizes our study.

2. Mathematical modeling

The cardiovascular-respiratory model depicted in Fig. 1 represents a lumped parameter compartmental model designed to predict patient-specific dynamics of cerebral CO_2 reactivity during hypercapnic breathing in a CHF patient. The model consists of two parts: a cardiovascular model that predicts the main quantity of interest cerebral vascular resistance R_B [mmHg s/ml], as well as systemic arterial blood pressure p_{Sa} [mmHg], middle cerebral blood flow velocity v_{MCA} [ml/s], and left ventricular ejection fraction EF. The cardiovascular model is coupled to a respiratory model that predicts expiratory CO_2 partial

pressure $p_{\text{exp,CO2}}$ [mmHg]. These quantities are predicted as a function of heart rate H [beats/s], airflow velocity $\dot{V}_{IE}$ [ml/s], and concentration of inspired CO_2 [ml_{stpd}/ml]. The model is designed to predict these quantities for a patient resting in semi-recumbent position. The test protocol involves two stages. The patient first breathes in normal air (approximately zero % CO_2) for 5 min after which a switch to hypercapnic air containing 5% CO_2 is made. This switch in CO_2 concentration is modeled by dynamically changing the concentration of inspired CO_2. The inducement of hypercapnia elicits autonomic and autoregulatory control responses. Autonomic responses to the CO_2 challenge include changes in heart rate, breathing depth and frequency, and minor changes in cardiac contractility and systemic vascular caliber. Effects on the first two quantities (heart rate and airflow) are directly incorporated as model inputs, while the autonomic control quantities (contractility and systemic vascular resistance) are not included in the model. The main autoregulatory response to the CO_2 challenge is regulation of the vessel caliber in the cerebral vasculature. This key response is modeled via prediction of dynamic changes of the cerebral vascular resistance and represents a measure of cerebral CO_2 reactivity. Below, we describe the basic cardiovascular and respiratory models, as well as nominal parameter values. All model quantities are defined in cgs units (cm, grams, and seconds), with the exception of pressure, which is computed in mmHg, standard for the physiology literature.

2.1. Cardiovascular model

The cardiovascular system (see Fig. 1) is represented by a closed circuit with 3 arterial compartments, 3 venous compartments, and 2 ventricular compartments. Vascular compartments represent systemic arteries and veins in the body and the brain, as well as pulmonary arteries and veins. Each compartment lumps related vessels yielding a representative transmural pressure $p(t)$ [mmHg], volume $V(t)$ [ml], compliance C [ml/mmHg] (constant). Compartments are separated by resistors R [mmHg s/ml], analogous to an RC-circuit. The physiological analogy of compliance is vascular tone, while resistances can be predicted from vascular caliber through Poiseuille's law for flow in a cylinder, where resistance R is inversely proportional to the radius r to the fourth power, $R = k/r^4$. It should be noted that each compartment lumps many vessels together, thus a direct computation relating radius to resistance is not feasible.

For each compartment i, the stressed volume $V_{i,str}(t)$ [ml] is given by

$$V_{i,str}(t) = V_i(t) - V_{i,unstr} = C_i p_i(t), \quad (1)$$

where $V_i(t)$ [ml] is the time-dependent total volume and $V_{i,unstr}$ [ml] (constant) is the unstressed volume, at zero transmural pressure.

Flows between adjacent compartments are characterized by a constant resistance R [mmHg s/ml] and volumetric flow rate $q(t)$ [ml/s]. Incorporating Ohm's law, the net change in volume for each compartment is given by

$$\frac{dV_i(t)}{dt} = q_{in}(t) - q_{out}(t), \; q_{in}(t) = \frac{p_{i-1}(t) - p_i(t)}{R_{in}}, \; q_{out}(t) = \frac{p_i(t) - p_{i+1}(t)}{R_{out}}, \quad (2)$$

The subscripts $i-1$ and $i+1$ refer to upstream and downstream compartments in relation to compartment i, respectively. A system of differential equations is obtained by differentiating (1) and equating with (2) to give

$$\frac{dp_i(t)}{dt} = \frac{q_{in}(t) - q_{out}(t)}{C_i}. \quad (3)$$

An equation of this form is associated with each vascular compartment.

The heart is represented by the left and right ventricles, modeled to generate the driving pressures for the systemic and pulmonary systems, respectively. This is realized by imposing a time-varying pressure as a function of ventricular volume. Thus, for the ventricular compartments V_{iv} we obtain a differential equation by imposing volume conservation, as

$$\frac{dV_{iv}(t)}{dt} = q_{in}(t) - q_{out}(t), \quad i = l, r, \quad (4)$$

where the flows $q(t)$ [ml/s] are determined similarly to (2). We use a time-varying elastance model to compute ventricular pressures $p_{iv}(t)$ [mmHg] [12, 13, 14, 15],

$$p_{iv}(t) = E_{iv}(t)\left[V_{iv}(t) - V_{id}\right], \quad i = l, r, \quad (5)$$

where V_{id} [ml] denotes the volume at zero end-systolic pressure [12, 16] and $E_{iv}(t)$ [mmHg/ml] denotes the time-varying elastance. In the above equations subscript i denotes the left or right ventricle, respectively. For each ventricle, time-varying elastance $E(t)$ [mmHg/ml] is modeled using a piecewise sinusoidal function of the form

$$E(t) = \begin{cases} (E_S - E_D)\left[1 - cos\left(\frac{\pi t}{T_M}\right)\right]/2 + E_D & 0 \le t \le T_M \\ (E_D - E_D)\left[cos\left(\frac{\pi(t - T_M)}{T_R}\right) + 1\right]/2 + E_D & T_M \le t \le T_M + T_R \\ E_D & T_M + T_R \le t \le T, \end{cases} \quad (6)$$

where T_M and T_R [s] denote the time for end-systolic (maximum) elastance (T_M) and the remaining time to relaxation (T_R). To account for varying heart rate, we express these times as fractions of the heart period $T = 1/H$[s], i.e., $T_{M,f} = T_M/T$ and $T_{R,f} = T_R/T$. We assume that maximum elastance occurs at the same time for both left and right ventricles, thus the values of the two parameters T_M and T_R [s] remain the same for the two sides of the heart. E_D and E_S [mmHg/ml] denote the end-diastolic and end-systolic elastance of each ventricle. The elastances differ significantly between the right and the left ventricle, in particular for the CHF patient studied in this manuscript. Thus we include four elastance parameters $E_{D,l}, E_{D,r}$ and $E_{S,l}, E_{S,r}$ [mmHg/ml] and two timing parameters T_M and T_R [s].

Similar to previous studies [17, 18, 19], the cardiac valves (mitral mv, aortic av, tricuspid tv, and pulmonary pv) are modeled using time-varying resistances $R_{mv}(t)$, $R_{av}(t)$, $R_{tv}(t)$, $R_{pv}(t)$ [mmHg s ml] defined as a function of the pressure drop across the valves. A small baseline resistance is used to define an "open" valve (subscript "o") and a resistance that is several orders of magnitude larger is used to define the "closed" valve (subscript "c"). An

exponential function is applied to describe the degree of openness as a function of the pressure gradient. Thus the effective resistance of a valve is defined by

$$R_{valve}(t) = min\left[R_{valve,o} + e^{-k(p_{in}(t)-p_{out}(t))}, R_{valve,c}\right]. \quad (7)$$

The parameter *Rvalve,o* [mmHg s/ml] is the small resistance allowing flow out of the ventricle, *k* describes the speed of the transition from open to closed, and *Rvalve,c* [mmHg s/ml] is a value large enough to effectively shut off the flow through the valve. Since this function is non-smooth at the junctions of the exponential and *Rvalve,c*, a smoothing function [20] was used. A smooth minimum can be computed as

$$min_{\varepsilon}(x) = -\varepsilon\, log\left(\sum_i exp\left(-x_i/\varepsilon\right)\right), \quad (8)$$

where $0 < \varepsilon < 1$ denotes the degree of smoothness (in this study we used $\varepsilon = 0.5$) and x denotes the vector to be minimized. Similarly, a smooth maximum could be computed as $\max_e(x) = -\min_{\varepsilon}(-x)$.

Cerebral autoregulation, activated during the switch from eucapnic to hyper-capnic breathing, causes cerebral vasodilation, i.e., the caliber and consequently the resistance of vessels in the cerebral vasculature decreases. This decrease in cerebral vascular resistance causes an increase in cerebral blood flow velocity as observed in measurements of associated data (see Fig. 6). Similar to previous studies [17], we included cerebral autoregulation by modeling peripheral vascular resistance in the brain as a piecewise linear function in time of the form

$$R_B(t) = \sum_{i=1}^{n} \gamma_i H_i(t),$$
$$H_i(t) = \begin{cases} \frac{t-t_{i-1}}{t_i-t_{i-1}}, & t_{i-1} \le t_i \\ \frac{t_{i+1}-t}{t_{i+1}-t_i}, & t_i \le t_{i+1} \\ 0, & \text{otherwise}, \end{cases} \quad (9)$$

where the unknown function values at nodes γ_i are model parameters.

The input to the cardiovascular model is the period of the cardiac cycle $T = 1/H$, which is obtained from data (see Fig. 2). Note, that this period is not constant but varies with each cardiac cycle. Four quantities constitute the model output, the first being the cerebral vascular resistance (the resistance in the brain, R_B) as described above. Three additional output quantities are compared with the model data. Systemic arterial blood pressure p_{Sa} is found from the solution of the differential equation (28). Blood flow velocity in the middle cerebral artery v_{MCA} is related to the total flow to the brain by

$$v_{MCA} = \frac{q_B}{\kappa}, \quad q_B = \frac{p_{Ba} - p_{Bv}}{R_B},$$

where κ is a scaling factor relating volumetric blood flow in the brain to blood flow velocity measured in the middle cerebral artery. We assume that this factor is constant, implying that

no active changes in vessel properties (diameter and vascular tone) occur at the level of the major cerebral arteries. The final output is the ejection fraction

$$EF = \frac{V_{lv,max} - V_{lv,min}}{V_{lv,max}},$$

where $V_{lv,max}$ and $V_{lv,min}$ are the maximum and minimum volume of the left ventricle, respectively. Note, since the ventricular volume is a dynamic quantity, the maximum and minimum volumes change over each cardiac cycle. To ensure differentiability, these quantities are computed as smooth minimums and maximums from V_{lv} (one of the state variables) using the smoothing function (8).

All equations for the cardiovascular model are given in Appendix A.1, and parameterization is discussed in the beginning of Section 2.3.

2.2. Respiratory model

The respiratory system (also depicted in Fig. 1) contains tissue and lung com partments. Metabolism, defined here as the consumption of O_2 and production of CO_2, occurs in all tissue and organs. We lump tissue and organs in the same compartment, but divide the mass into two regions: brain tissue *B* and systemic tissue *S*. These two regions are each divided into two compartments: a tissue compartment *tis* where metabolic activity resides and an interfacing capillary compartment *cap* where gas exchange between tissue and blood occurs, see e.g., [21]. The lungs, where O_2 and CO_2 are exchanged with the environment, are described by an alveolar compartment and three dead space compartments. Standard material balance equations describe the exchange of gases within each compartment and between the tissue compartments and interfacing capillaries.

Tissue equations—The following symbol convention will be used: *c* represents concentration [ml_{gas}/mlblood], subscript *T* represents a generic tissue compartment which can be chosen to be systemic *S* or brain *B* tissue, generic gas quantities (O_2 or CO_2) are denoted by *g* and the gas fractional amount by *F*. Venous flow [ml/s] is denoted by v and arterial flow [ml/s] by *a*. Following this symbol convention, and as mentioned above, we distinguish between two tissue-related compartments: the actual tissue regions *Ttis* denoted as *Stis* and *Btis*, and the capillary blood compartments *Tcap* denoted as *Scap* and *Bcap*. The latter compartments serve as an interface between the tissue compartments and the blood stream. The two tissue compartments are marked in yellow on Fig. 1, while the systemic and brain capillary compartments are indicated as expansions where arteries and veins intersect.

Let the general quantity of a gas *g* (O_2 or CO_2) in a tissue region *T* (*B* or *S*) be written as $A_{T,g}$, then, the total amount of a gas in a tissue region $A_{T,g}$ [ml] can be found as

$$A_{T,g} = V_{T,g} C_{T,g}. \quad (10)$$

This equation describes $A_{T,g}$ [ml] as the product of the effective tissue volume *V* [ml] (constant) available for the gas and the concentration *c* [ml_{gas}/mlvolume] of the gas in the volume.

The change in the amount of gas g in the tissue compartment depends on the amount of gas produced or consumed by metabolism $M_{T,g}$ [ml/s] and the amount added or removed by exchange through diffusion with the capillary compartment. Similarly, the change in the amount of gas in the capillary compartment depends on the removal of gas by the bloodstream q_T [ml/s] and diffusion of gas into or out of the tissue compartment, i.e., by differentiating (10) we obtain

$$\begin{aligned}\frac{dA_{Ttis,g}}{dt} &= \frac{dV_{Ttis,g}}{dt}c_{Ttis,g}+V_{Ttis,g}\frac{dc_{Ttis,g}}{dt}\\ &= M_{T,g}-D_{T,g}\left(c_{Ttis,g}-c_{Tcap,g}\right),\\ \frac{dA_{Tcap,g}}{dt} &= \frac{dV_{Tcap,g}}{dt}c_{Tcap,g}+V_{Tcap,g}\frac{dc_{Tcap,g}}{dt}\\ &= q_{T,g}\left(c_{a,g}-c_{Tcap,g}\right)+D_{T,g}\left(c_{Ttis,g}-c_{Ttis,g}-c_{Tcap,g}\right).\end{aligned}$$

In the above equations, $D_{T,g}$ denotes the diffusion capacity for a gas in a given tissue (depending on partial pressure or concentration of the gas). $V_{Ttis,g}$ is the effective tissue volume for a gas, $V_{Tcap,g}$ is the effective capillary blood volume for a gas (approximately 1% of $V_{Ttis,g}$), and $q_{T,g}$ is the blood flow through the capillary compartment. The concentration in the arteries traveling to both the systemic circulation and the brain are the same since no metabolic effects are introduced until exchanges occur between capillary and tissue compartments. Hence we denote the arterial concentration for both regions as $c_{a,g}$ [$\text{ml}_{\text{gas}}/\text{ml}_{\text{blood}}$].

Assuming $dV_{T,g}/dt = 0$, the above equations reduce to generic equations predicting exchange between the tissue compartment and capillary blood combined with metabolism

$$V_{Ttis,g}\frac{dc_{Ttis,g}}{dt}=M_{T,g}-D_{T,g}\left(c_{Ttis,g}-c_{Tcap,g}\right) \quad (11)$$

and exchange between capillary blood and the tissue compartment combined with transport via the bloodstream

$$V_{Tcap,g}\frac{dc_{Tcap,g}}{dt}=q_T\left(c_{a,g}-c_{Tcap,g}\right)+D_{T,g}\left(c_{Ttis,g}-c_{Tcap,g}\right). \quad (12)$$

Assume that tissue compartments can be considered well-mixed and gas concentrations are equilibrated with exiting venous concentrations. Then the gas concentration $c_{v,g}$ [$\text{ml}_{\text{gas}}/\text{ml}_{\text{blood}}$] in the systemic venous return can be calculated as a mixture of the concentrations from the incoming systemic stream q_S [ml/s] and cerebral venous stream q_{Bv} [ml/s] as

$$c_{v,g}=\frac{c_{Stis,g}q_S+c_{Btis,g}q_{Bv}}{q_S+q_{Bv}},$$

where $c_{S,g}$ and $c_{B,g}$ [$\text{ml}_{\text{gas}}/\text{ml}_{\text{blood}}$] are the systemic and cerebral concentrations of each gas exiting the capillary compartments.

Lung equations—The lungs (also depicted on Fig. 1) are modeled using five compartments including pulmonary capillaries, the alveolar space, and three dead space compartments representing the bronchial airways. The compartment representing the alveolar space has a dynamic volume $V_{A,g}$, in which O_2 and CO_2 are exchanged between the lungs and the pulmonary capillaries. Let A denote the alveolar compartment; then the amount of alveolar gas is given by

$$V_{A,g} = V_A F_{A,g},$$

the product of alveolar volume V_A [ml] and gas fraction $F_{A,g}$. The change in quantity of alveolar gas is represented by a mass balance relation parallel to the one developed for the tissue compartment, taking into account a time-varying alveolar volume. Gas transport is via blood flowing to and from the lungs through pulmonary capillaries, and gas exchange with the environment is carried out via inspiration and expiration. A separation into lung tissue and lung capillary compartments is not included given the rapid and complete loading and unloading of blood gases between the alveoli and the the blood flow through the capillaries surrounding each alveolus. Note that the systemic venous return concentration $c_{v,g}$ will be the same as the pulmonary arterial concentration and systemic arterial concentration $c_{a,g}$ will be the same as pulmonary venous return. Thus, $c_{v,g}$ and $c_{a,g}$ are used to denote the pulmonary arterial and venous concentrations, respectively.

The bronchial airways have been modeled using a rigid anatomical dead space connecting the alveolar space with the atmosphere. This space is divided into three equal-volume compartments which each account for some of the effects of the pulmonary branching. We assume that the compartment marked D_1 is located closest to the mouth with the compartment marked by D_3 closest to the alveolar space. Gas concentrations and partial pressures are predicted in all compartments.

Following these considerations, the mass balance equation for the alveolar compartment can be written as

$$\frac{dV_{A,g}}{dt} = F_{A,g}\frac{dV_A}{dt} + V_A\frac{F_{A,g}}{dt} = \frac{dV_A}{dt}F_{i,g} + q_P\nabla\left(c_{v,g} - c_{a,g}\right).$$

In the above equation, subscript p marks the pulmonary compartment and $F_{i,g}$ marks the fraction of gas in the air that is either being inspired into or expired from the alveolar compartment. Hence, $i = D_3$ during inspiration since inspired air is coming from the adjacent dead space region and $i = A$ during expiration since air leaving the alveoli is alveolar air equilibrated with the pulmonary capillaries. Rearranging to express the rate of change of alveolar gas fraction gives

$$V_A\frac{dF_{A,g}}{dt} = \begin{cases} \frac{dV_A}{dt}\left(F_{D_3,g} - F_{A,g}\right) + q_P\left(c_{v,g} - c_{a,g}\right), & \text{inspiration} \\ q_P\left(c_{v,g} - c_{a,g}\right), & \text{expiration.} \end{cases}$$

To convert gas fractions to partial pressures (in mmHg) and maintain consistency of units we use the the relationship

$$F_{A,g} = \frac{p_{A,g}}{(p_{amb} - p_{water})} = \frac{p_{A,g}}{713}, \quad (13)$$

where p_{amb} is the ambient air pressure of 760 mmHg and water vapor partial pressure p_{water} equals 47 mmHg at body temperature of 37 °C. Because blood gas concentrations are reported in [ml_{stpd}/ml] ("standard temperature pressure dry"), but alveolar volumes are in btps ("body temperature pressure saturated"), we convert tissue concentrations to btps. One assumption included here is that incoming air is immediately humidified once it enters the nasal passages [22, 23] and that expired air is a composition of alveolar air and dead space air at btps, therefore terms with those quantities are not converted.

Additional modeling considerations concern the relationship between the pulmonary capillaries and the systemic arteries. First, the effective amount of blood in contact with alveolar air is reduced by blood bypassing alveoli and can also be reduced by under-ventilated alveoli. A 2% anatomical shunt is assumed for blood bypassing the alveoli, appropriate for an adult with no known anatomical abnormalities [22, 23]. As a consequence, only 98% of the cardiac output becomes oxygenated, and we alter the alveolar equations accordingly. We note that physiologically, the amount of blood not in effective content with alveolar air can range from 2-5% [22, 23], with the lower end of the range for healthy subjects and the higher end indicating a pathological condition, such as collapsed or obstructed lungs and congenital cardiovascular conditions. Since the subject analyzed here has no known pulmonary or congenital cardiovascular disease associated with CHF, using a 2% shunt is justified. This appears in (14) as the factor 0.98.

Second, we note that the thin alveolar wall allows for almost immediate equilibration of gases between the alveoli denoted by *A* and the pulmonary capillaries; thus we assume that the concentrations of blood gases are the same in the pulmonary capillaries and in the systemic arteries. Thus, in terms of partial pressures we have $p_{A,g} = p_{a,g}$ as an auxiliary equation. Intermediate equations taking into account the modeling considerations and unit conversions discussed above are presented previously in Ellwein [24], with the final alveolar equations given as

$$V_A \frac{dp_{a,g}}{dt} = \begin{cases} \frac{dV_A}{dt}\left(p_{D_3,g} - p_{a,g}\right) + 0.98 \cdot 863\, q_P\, (c_{v,g} - c_{a,g}), & \text{inspiration} \\ 0.98 \cdot 863\, q_P\, (c_{v,g} - c_{a,g}), & \text{expiration.} \end{cases} \quad (14)$$

Each of the three compartments making up the anatomical dead space is considered to be well-mixed with units V_{btps}, in ml. Material balance equations for the dead space compartments reflect changes in gas levels due to airflow, with opposite directions of flow for inspiration versus expiration. The relation (13) holds and equation units are all in btps. Thus following the derivation of (14),

$$\text{Inspiration:} \quad \begin{aligned} V_{D_1} \frac{dp_{D_1,g}}{dt} &= \frac{dV_A}{dt}\left(p_{I,g} - p_{D_1,g}\right), \\ V_{D_i} \frac{dp_{D_i,g}}{dt} &= \frac{dV_A}{dt}\left(p_{D_{i-1},g} - p_{D_i,g}\right), \quad i=2,3 \end{aligned} \tag{15}$$

$$\text{Expiration:} \quad \begin{aligned} V_{D_i} \frac{dp_{D_i,g}}{dt} &= \frac{dV_A}{dt}\left(p_{D_i,g} - p_{D_{i+1},g}\right), \quad i=2,3 \\ V_{D_3} \frac{dp_{D_3,g}}{dt} &= \frac{dV_A}{dt}\left(p_{D_3,g} - p_{a,g}\right). \end{aligned} \tag{16}$$

In the above equations, pressure $p_{I,g}$ [mmHg] denotes the partial pressure of the gas in the inspired air.

O_2 and CO_2 have different affinities for hemoglobin, and therefore behave differently as gases in the air versus dissolved in blood. Gas dissociation laws are used as auxiliary equations to convert alveolar gas pressures to blood gas concentrations. In this study we use equations presented in Batzel et al. [1],

$$\begin{aligned} c_{T,CO_2} &= K_{CO_2} p_{T,CO_2} + k_{CO_2}, \\ c_{T,O_2} &= K_{O_2}\left(1 - e^{-k_{O_2} p_{T,O_2}}\right)^2. \end{aligned}$$

The linear law for CO_2 and the exponential law for O_2 are empirical relationships reflecting the general behavior of each gas, but do not explicitly model gas interdependencies or factors such as pH and temperature.

Inputs for the respiratory model include heart rate and flows predicted by the cardiovascular model as well as inspired volumetric airflow $\dot{V}_{IE}$ [ml/s] measured during experimentation. Note, $\dot{V}_{IE}$ is equivalent to the rate of change of alveolar volume $dV_{T,g}/dt$ [ml/s]. Thus, the alveolar volume can be predicted as

$$V_A = \int \dot{V}_{IE}\, dt. \tag{17}$$

The integration constant is chosen such that the minimum alveolar volume matches the functional residual capacity (FRC) [ml] estimated as a function of height h [cm] and weight w [kg] [25], i.e.,

$$min\,(V_A) = FRC, \quad FRC = (3.8\,h/100 - 3.41\,w/h - 2.74)\,1000.$$

Note that dV_A/dt [ml/s] is positive during inspiration and negative during expiration.

The second input to the respiratory model is the partial pressure of inspired CO_2 ($p_{\text{insp, CO2}}$) determined by estimating a smooth curve through the minima of the expired CO_2 values from experimental data as shown on Fig. 2. The minimum CO_2 level occurs during inspiration, both for inspired normal air and for inspired air with elevated CO_2. In both cases expired air includes the inspired CO_2 plus the quantity of higher-concentration CO_2 generated from metabolism and transferred to alveolar air through the alveolar-capillary

exchange. Note, the data automatically includes the switch from eucapnic to hypercapnic breathing.

Only one model output is predicted from the respiratory model, namely, expiratory CO_2 partial pressure (p_{expCO2}), which is computed as

$$p_{exp,CO_2} = f_{alv} p_{a,CO_2} + (1 - f_{alv})\, p_{D_1,CO_2}.$$

Expiratory partial pressures are assumed to be nearly equivalent to the dead space pressure in D_1 closest to the mouth, with a slight mixing of alveolar gas. Thus the factor f_{alv} is introduced to represent the fraction of alveolar gas convected into the expired mixture. For model comparison, $p_{\text{exp,CO2}}$ is compared to the data for expiratory CO_2 partial pressure. All respiratory equations are listed in Appendix A.2, while parameterization is discussed beginning in Section 2.3.

2.3. Parameterization

2.3.1. Nominal cardiovascular parameters—Nominal parameter values and initial conditions for the cardiovascular model were calculated from data, literature, and using the subject's anthropometric measurements. Parameter values used to predict time-varying elastance include endsystolic and end-diastolic elastance of the left ventricle ($E_{S,i}$,$E_{D,i}$, $i = l,r$) [mmHg/ml], as well as fractions denoting the timing of the cardiac cycle ($T_{M,f}$,$T_{R,f}$). Values for the end-diastolic elastance are obtained from estimated diastolic ventricular pressure p_{dia}, end-diastolic volume EDV, and zero pressure volume V_d [ml] as

$$E_{D,i} = \frac{p_{i,dia}}{EDV_i - V_{d,i}}, \quad i = l, r, \quad (18)$$

where the diastolic ventricular pressures are set using literature values [26]. The subject studied has CHF and is thus expected to have an enlarged left ventricle, while the size of the right ventricle is closer to normal. We estimate these volumes using results for CHF patients without sleep apnea reported by Tkacova et al. [27].

End-systolic elastances are estimated using a similar relation, but as a function of systolic ventricular pressure p_{sys} [mmHg], end-systolic volume ESV [ml], and zero pressure volume V_d [ml]. Systolic ventricular pressure is obtained from the maximum measured arterial pressure. End systolic volume ESV [ml] is obtained by subtracting stroke volume (SV [ml beat]) from the end-diastolic volume (EDV), while the stroke volume is estimated from end left ventricular diastolic volume and ejection fraction (EF, measured 26% for the subject studied):

$$ESV = EDV - SV, \quad SV = EF \cdot EDV_{lv}. \quad (19)$$

The timing fractions $T_{M,f}$ and $T_{R,f}$ were estimated from literature values suggested by Ottesen and Danielsen [28] and Heldt [29]. We assume that the ejection of the left and the right sides of the heart are synchronous, thus we use the same values for both ventricles.

Total blood volume (ml) was computed using Baker's formula [30] as a function of body surface area (BSA (m^2), estimated from Mosteller's formula [31]) again as a function of height h [cm] and weight w [kg]:

$$V_t = (23.9 \cdot BSA - 1.229)\,1000, \quad BSA = \sqrt{wh/3600}. \quad (20)$$

Distributions of volume and unstressed volumes were obtained using values from Beneken and DeWitt [32].

Mean flows were scaled to cardiac output, which was computed from stroke volume SV and mean heart rate $\bar{H}$ [beats/s] [26], i.e.,

$$CO = SV \cdot \overline{H}, \quad (21)$$

where the mean heart rate was obtained from the measurements. Flows in the circuit were distributed to reflect a 20% cardiac output distribution to the brain, while 80% was directed to the systemic arteries [23, 26].

Mean pressures were obtained from literature values [26, 23] and scaled using available data. Scaling was done such that left ventricular systolic pressure was set to the maximum measured arterial pressure, while the mean systemic arterial pressure were predicted by calculating the mean over the part of the time-series representing eucapnic breathing. We assumed a negligible drop in arterial pressure (1%) between arterial pressure in the aorta and the main arteries in the cerebral vasculature, i.e., $p_{Ba} = 0.99 p_{Sa}$.

Resistors were determined using Ohm's law (2) while values for compliances were obtained from a pressure volume relation (1). Both were predicted using mean values for pressure, flow, and volume, i.e.,

$$R_i = \frac{\overline{p}_{in} - \overline{p}_{out}}{\overline{q}_i}, \quad C_i = \frac{V_{str,i}}{\overline{p}_i}, \quad (22)$$

where stressed volumes for each compartment were determined using values given in the study by Beneken and DeWitt [32].

Finally, the scaling factor $\kappa = v_{\mathrm{MCA}}/qB$ relating the model output to the volu-metric flow rate computed by the model is predicted from literature values of diameters of the major cerebral arteries [33]. It should be noted that v_{MCA} represents the velocity of the left middle cerebral artery, while q_B represents the volumetric flow to the entire brain, i.e., through all cerebral arteries. Assuming that the major cerebral arteries do not change their diameter or vascular tone, the scaling factor will be constant.

Initial conditions for blood pressures and ventricular volumes used for the differential equations were obtained partly from the data and partly from literature estimates. Initial conditions for arterial pressures were scaled relative to the mean of the measured arterial pressure (as discussed above) assuming that the pressure drop over the larger arteries is

small, while initial conditions for venous pressures and the ventricular volumes were were set using standard literature estimates [23, 26].

In summary, the cardiovascular model contains 24 parameters including 9 resistances $R = \{R_S, R_B, R_{Ba}, R_{B1}, R_P, R_{mv,o}, R_{av,o}, R_{tv,o}, R_{pv,o}\}$, 6 compliances $C = \{C_{Sa}, C_{S1}, C_{Ba}, C_{B1}, C_{Pa}, C_{pv}\}$, 8 heart parameters $\theta_{heart} = \{V_{dl}, V_{dr}, E_{D,l}, E_{D,r}, E_{S,l}, E_{S,r}, T_M f, T_R f\}$, and the scaling factor κ. Nominal parameters and initial conditions for the differential equations are specified in the Appendix, Table 3.

2.3.2. Nominal respiratory parameters—Nominal respiratory parameters and initial conditions are obtained primarily from literature values scaled to the subject's weight and gender. As is standard practice, all tissue gas volumes and blood gas concentrations are given in stpd, thus units are consistent. Metabolic rates were set using standard allometric scaling proportional to body mass by the power of 3/4 [34, 35] using values in the Appendix, Table 4. We used the lumped metabolic rates for the systemic tissue given in [1, 36, 37] (scaled to the subject's weight and gender) for CO_2 ($M_{S,CO2}$) and O_2 ($M_{S,O2}$). These studies also report a lumped CO_2 metabolic rate for brain tissue ($M_{B,CO2}$). To get a metabolic rate for O_2 in the brain, we used the assumption suggested by Grodins et al. [37] that the brain O_2 metabolic rate is approximately equal to the metabolic rate for CO_2, i.e., we let $M_{B,O2} = M_{B,CO2}$. For the gas diffusion constants $D_{T,g}$, we used values given by Conrad et al. [21]. This study does not report differentiated values between brain and systemic tissue, thus we used the same constant for both organs and both blood gases and in addition the same volume ratio between tissue and capillary compartments for both CO_2 and O_2 systemic and brain compartments with capillary volume 1% of tissue volume.

Compartment volumes of the various gases were based on values in Batzel [1, 36, 37]. Alveolar volume is a dynamic quantity as shown in (17). Dead space volume was set proportional to the body weight, and the coefficients of the dissociation equations are assumed to be independent of the size of the subject.

Initial conditions for the differential equations were also obtained from literature values. For the alveolar and dead space space compartments initial conditions are given for partial pressures of CO_2 and O_2, respectively. Assuming that the first dead space compartment D_1 is closest to the mouth we assumed that the O_2 concentration in this compartment should be close to that of room air. Assuming a slight decrease in O_2 partial pressure as air is transported through the lungs we let $p_{D2,O2} = 158$ mmHg and $p_{D3,O2} = 157$ mmHg. The CO_2 partial pressure in inspired air is small. Using an average value extracted from the mean of inspired CO_2 data shown in Fig. 2, we chose initial conditions for partial pressures as increasing along the dead space using a similar logic as for oxygen (all initial values summarized in the Appendix, Table 4). These values also agree with those used by Grodins et al. and Khoo et al. [37, 38].

Partial pressure in the alveolar compartments were obtained from values suggested by [39, 40]. These values reflect magnitudes that are between values in inspired air and standard values reported in the lung. For systemic and brain tissue we used initial conditions reported

in [40, 37, 38]. Finally, to obtain initial conditions for the capillary compartments we assumed that the system was in steady state, thus we let

$$c_{Tcap,g} = c_{Ttis,g} - M_{T,g}/D_{T,g}. \quad (23)$$

In summary, the respiratory portion of the model contains 20 parameters, including 4 metabolic rates $M = \{M_{S,CO2}, M_{S,O2}, M_{B,CO2}, M_{B,O2}\}$, 4 gas tissue volumes $V = \{V_{Stis,CO2}, V_{Stis,O2}, V_{Btis,CO2}, V_{Btis,O2}\}$ and 4 gas capillary volumes $V = \{V_{Scap,CO2}, V_{Scap,O2}, V_{Bcap,CO2}, V_{BcapO2}\}$, the lung dead space volume V_D, 4 dissociation constants $K = \{K_{O2}, k_{O2}, K_{CO2}, k_{CO2},\}$, two diffusion constants $D_{T,CO2}$ and $D_{T,O2}$, a parameter allowing us to predict gas volume in the capillary compartment $f_{V,cap}$, and a fraction f_{alv} indicating alveolar air in the exiting air stream. Nominal parameter values and initial conditions for the differential equations are specified in the Appendix, Table 4.

3. Experimental methods

The data analyzed in this study include continuous measurements (sampled at 128 Hz) of heart rate H [beats/min], systemic arterial blood pressure (p_{Sa} [mmHg]), cerebral blood flow velocity v_{MCA} [cm/s] measured from the middle cerebral artery (MCA), inspired volumetric airflow V_{IE} [ml/s], and expired partial pressure of CO_2 [mmHg]. In addition we have a measure for left ventricular ejection fraction (EF), as well as anthropometric measurements of height, weight, and gender. These data are obtained from the Pulmonary Physiology Laboratory, Middleton Veterans Hospital, Madison WI. Detailed descriptions of the experimental protocol can be found in [6] but are also summarized below.

Time series data were analyzed from one subject diagnosed with CHF and no sleep apnea syndromes. This subject is a 55 years old male, height 178 cm, weight 82.3 kg with an ejection fraction of 26%. Two breathing protocols were analyzed 1: Eucapnia, denoting the state that the subject breathes room air at room temperature, and 2: Hypercapnia, denoting the state that the subject breathes a constant mixture of air containing 5% CO_2. Under both breathing protocols, the subject was resting in a semi-recumbent position with the head still and eyes open. When steady state signals were observed, eucapnic data were recorded for 250 s. At this point, the CO_2 challenge was initiated and another 250 s of data were recorded during hypercapnia.

To obtain data, the subject was instrumented with a 2-MHz pulsed Doppler ultrasound system (Neurovision 500 M; Multigon Industries, Yonkers, NY) used to continuously measure cerebral blood flow velocity in the proximal segment of the middle cerebral artery (MCA). The MCA was insonated through the right temporal bone window using search techniques described in Otis and Ringelstein [41]. After detection and optimization of the Doppler signal, the probe was mechanically secured using a headband device and probe holder to provide a fixed angle of insonation for the duration of the experiment. The subject was asked to keep his head still and eyes open throughout the experiment. Heart rate was obtained from the electrocardiogram, and arterial pressure (p_{Sa} [mmHg]) was measured beat by beat in the middle finger of the left hand by photoelectric plethysmography (Finapres, Ohmeda, Louisville CO). Inspired volumetric airflow was measured with a

pneumotachograph Model 3700, Hans Rudolph, Kansas City, MO) that was attached to a leak-free nasal mask. Expiratory CO_2 partial pressure ($p_{exp,CO2}$ [mmHg]) was sampled from the mask and measured by gas analyzers (#S-3A/I & CD-3; Ametek, Pittsburgh PA). Left ventricular ejection fraction was measured using two-dimensional echocardiography with a Hewlett-Packard echocardiography device (SONOS model 5000).

4. Patient-specific model adaptation

In order to render the model patient-specific, model parameters are estimated to minimize the least squares error between computed and measured values of arterial pressure p_{Sa}, cerebral blood flow velocity v_{MCA}, left ventricular ejection fraction EF, and expiratory CO_2 partial pressure. Similar to previous studies [19, 24] we note that to accurately reproduce cardiovascular dynamics it is important to account for both instantaneous as well as systolic and diastolic values of arterial pressure and cerebral blood flow velocity. The quantities (pressure, velocity, partial pressure of CO_2) are observed at N equally spaced times t_i, according to the frequency of data collection (128 Hz). Similarly, for arterial pressure and cerebral blood flow velocity we have one observation of systolic and diastolic pressure for each of M cardiac cycles. In addition, we have an average value for ejection fraction EF during eucpania.

Each of the predicted model outcomes has an associated data vector, which we denote a superscript (d). Consequently, the data vectors are p^d_{Sa}, v^d_{MCA}, $p^d_{Sa,sys}$, $p^d_{Sa,dia}$, $v^d_{MCA,sys}$, $p^d_{MCA,dia}$, EF^d and p^d_{exp,CO_2}. To calculate the least squares error, we define two residual vectors $\mathbf{R}_{car}$ and $\mathbf{R}_{resp}$, containing quantities relevant for the cardiovascular and respiratory models, respectively:

$$\begin{aligned}\mathbf{R}_{car}(t) &= \left[r_{p_{Sa}}, r_{v_{MCA}}, r_{p_{Sa,sys}}, r_{p_{Sa,dia}}, r_{v_{MCA,sys}}, r_{v_{MCA,dia}}, r_{EF}\right]^T \\ \mathbf{R}_{resp}(t) &= \left[r_{p_{exp,CO_2}}\right]^T,\end{aligned} \tag{24}$$

where each component is scaled to account for the number of elements in the vector and relative to the data, i.e.,

$$r_i(t) = \frac{1}{\sqrt{K}}\left[\frac{r_i(t_1) - r_i^d(t_1)}{r_i^d(t_1)}, \ldots, \frac{r_i(t_K) - r_i^d(t_K)}{r_i^d(t_K)}\right]^T,$$

with $i = p_{Sa}, v_{\mathrm{MCA}}, p_{Sa,sys}, p_{Sa,dia}, \ldots, p_{\mathrm{exp,CO2}}$, and $\kappa = N, M$, respectively.

The vector $\mathbf{R}_{car}$ has $2N + 5M$ entries, while $\mathbf{R}_{resp}$ has N entries. For each of the residual vectors $\mathbf{R}j$, the least squares cost J is defined by

$$J = \|\mathbf{R}_j\|_2^2 = \mathbf{R}_j^T \mathbf{R}_j, \quad j = car, resp. \tag{25}$$

Actual parameter estimates were predicted using nonlinear optimization, performed using log-scaled parameters to facilitate convergence:

$$\tilde{\theta}_{opt}=arg \quad min_{\tilde{\theta}}\, J\,(\theta)\,,$$

where $\tilde{\theta}=log\,(\theta)$.

Before solving the least squares problem we used sensitivity analysis and subset selection to identify parameter sensitivity and correlations among model parameters. The two models are coupled loosely: the cardiovascular model does not depend on the respiratory model, but the respiratory model depends on flows predicted by the cardiovascular model. During eucapnia, the flows do not change significantly, consequently mean flows were computed and input to the respiratory model. During hypercapnia, the flows change in response to the CO_2 challenge and thus the fully coupled model were solved at this stage. The process used for model simulations is illustrated in Fig. 3.

4.1. Eucapnia

During eucapnia the subject is resting in semi-recumbent position thus autonomic and cerebral autoregulation has limited effect. As a result, the cardiovascular and the respiratory models can be treated as two separate entities. The cardiovascular model is given heart rate as an input and via solution of Eqs. (27-28) model output is computed. The respiratory model depends on blood flow through the pulmonary, systemic and brain tissue regions. Moreover, respiratory oscillations are about 4-5 times slower than cardiovascular oscillations due to the cardiac cycle [26]. As a result the respiratory dynamics are not expected to change significantly. Consequently, mean values can be computed from the cardiovascular model and input to the respiratory model.

Simulations done under eucapnia are set up to reflect dynamics of a resting subject. Data were collected after the subject had rested for a period of time until stable signals were obtained. The cardiovascular model has fast dynamics, consequently, impact of approximated initial conditions will die out quickly and the model will settle oscillating around steady state. However, the volume of the systemic tissue compartment is large, and as discussed by Farhi [42] it can take more than an hour for the systemic tissue CO_2 to be in steady state. To account for the tissue gas time scale being an order of magnitude longer than the 250 s of eucapnic data, we performed model analysis of steady state dynamics with the last 250 s segment of an extended data set created by replicating the eucapnic data 40 times. Figure 4 shows dynamics of the cardiovascular and respiratory data as a function of time, with the cardiovascular system reaching steady state oscillations within a few seconds, while the respiratory system takes more than an hour to reach steady state.

4.1.1. Sensitivity analysis—Sensitivity analysis gives a measure of how much the output of a model is affected by changes in the model parameters [18]. For the system discussed here, sensitivities were computed during eucapnia analyzing how sensitive the model output (arterial blood pressure, p_{Sa}, cerebral blood flow velocity v_{MCA}, ejection fraction EF, and expiratory CO_2 partial pressure $p_{\mathrm{exp,CO}}$) are to the model parameters. Sensitivities were computed for the cardiovascular and the respiratory models separately. Since a number of

physiological quantities at several scales were included, sensitivities were computed from the Jacobian defined by

$$S_{j,\tilde{\theta}_i}(t) = \left.\frac{\partial \mathbf{R_j}(\theta)}{\partial \tilde{\theta}_i}\right|_{\theta=\theta_0}, \quad \text{for} \quad i=1,\ldots,n \quad \text{and} \quad j=car,resp, \quad (26)$$

where n denotes the number of parameters. Note that the Jacobian is calculated with respect to the log-scaled parameters $\tilde{\theta}$, limiting the effect of varying parameter scales, but the differential equations are evaluated at nominal parameter values θ_0. Sensitivities are local in the model parameters, i.e., if parameter values θ_0 are changed so will the sensitivities. Since the model is nonlinear, the impact of each parameter may change as the values of the model parameters θ_0 change. In the absence of an analysis of this large parameter space, not feasible within the scope of this study, we assume that for well-chosen nominal parameters θ_0 the local sensitivity predictions will persist over a reasonable range of parameter values.

Given that the model states are time-series, the sensitivities will be time-varying as well. However, during eucapnia, we expect both the solution and the sensitivities to oscillate around steady state values. Thus it it reasonable to use ranked sensitivities for comparing the impact of model parameters to the model output. To obtain ranked sensitivities we used the standard 2-norm scaled with the largest sensitivity, i.e.,

$$\overline{S}_{j,\tilde{\theta}_i} = \left\| S_{j,\tilde{\theta}_i}(t) \right\|_2 / max\left(S_{j,\tilde{\theta}}(t) \right), \quad j=car,resp \quad \text{and} \quad i=1,\ldots,n.$$

4.1.2. Subset selection—Solving the inverse problem uniquely is not feasible using the complex model combined with available data, since several combinations of parameters likely give rise to the same solution. To achieve a simpler inverse problem, we limit the set of parameters identified using subset selection to obtain a set of uncorrelated parameters. Numerous methods exist for estimating identifiable parameters as discussed in recent studies [43, 44]. In this study, we used a method based on QR factorization as outlined below. Further details of this method can be found in [19, 45].

Recall that $\tilde{\theta}$ is the vector of n log-scaled model parameters and $\mathbf{R}$ is the model residual defined in (24). The subset selection method analyzes the Jacobian, $\mathbf{R}'$ predicted using (26) to find a subset of columns that are “maximally independent”. Singular value decomposition is used to decompose the Jacobian $\mathbf{R}' = U\Sigma V^T$, such that Σ is a diagonal matrix containing the singular values $\sigma_1 \geq \sigma_2 \geq \ldots \sigma_n$ and V is an orthogonal matrix of corresponding right singular vectors. The number of identifiable parameter values is predicted by the numerical rank ρ of $\mathbf{R}'$, the largest value ensuring that $\sigma_\rho/\sigma_1 > \varepsilon$. For our study $\varepsilon = \sqrt{\varepsilon_S}$, where ε_S is the relative tolerance used to solve the differential equations. Using ρ, the matrix of eigenvectors V^T can be partitioned as $[V_\rho\, V_{n-\rho}]^T$. The parameters associated with the ρ highest singular values are then found using QR-decomposition with column pivoting. We first determine a permutation matrix P by $V_\rho^T P = QR$, where Q is an orthogonal matrix, and the first ρ elements of R form an upper triangular matrix with diagonal elements in decreasing order. Then P is used to reorder the parameter vector $\theta_{0,\rho} = P^T \theta_0$. This gives the

partition $\theta_0 = \{\theta_{0,\rho}, \theta_{0,\,n-\rho}\}$, where $\theta_{0,\rho}$ contains the ρ identifiable parameters. Unidentifiable parameters the vector $\theta_{0,\,n-\rho}$ were kept at their nominal parameter values during the parameter estimation. It should be noted that estimating only identifiable parameters does introduce bias in the computations, but reduces the variance and makes the estimation algorithm more robust [46, 47]. Furthermore, it should be noted that the QR decomposition is not unique but depends on the concrete implementation of the algorithm; however, the algorithm will return a set of identifiable parameters for a given ρ.

4.1.3. Parameter estimation—To estimate the subset of model parameters we used the Levenberg-Marquardt method, a trust-region variant of the gradient based Gauss-Newton optimization method. Parameter estimation involves minimizing the least squares cost J defined in (25). Gauss-Newton is an iterative method [48] that at each iteration uses a solution based on a local linear approximation to compute the next iterate. The theory supporting our method predicts convergence even when the initial parameter estimates are far from the solution, and rapid convergence near the solution.

4.2. Eucapnia followed by hypercapnia

As discussed above great effort was put into achieving a set of model parameters that allowed prediction of steady state dynamics (during eucapnia). As described in the beginning of Section 3, hypercapnia was introduced by changing inspired concentration of CO_2. The response to this change involves activation of the autonomic and cerebral autoregulatory control systems. The autonomic control system acts to increase heart rate and breathing depth and frequency. These changes are included via inputs to the model. Cerebral autoregulation responds via vasodilation decreasing cerebral vascular resistance. This change in cerebral vascular resistance was modeled by redefining the parameter R_B using the piece wise linear function defined in (9), where parameters are defined as the function values at nodes. These parameters were estimated in a second simulation with the cardiovascular model, minimizing the least squares error between predicted and measured values of cerebral blood flow velocity. Using the optimized values for R_B, we re-estimated the identifiable respiratory parameters minimizing the least squares error between computed and measured values of expiratory CO_2 partial pressure. It was necessary for the latter simulation to use the coupled model, since equations predicting respiratory dynamics depend on predicted flows which are no longer constant but change in response to cerebral autoregulation. Note that for simulations done during hypercapnia, subset selection was not repeated.

5. Results

The cardiovascular-respiratory model analyzed in this study is derived in Section 2 (see also Fig. 1). This model uses heart rate, air flow, and inspired CO_2 data as system inputs and predicts pulsatile responses including cerebral vascular resistance, arterial and venous pressures in the systemic and pulmonary systems, partial pressures of CO_2 and O_2 in the lungs, as well as concentrations of these gases in the cerebral and systemic tissues. Parameter estimation is carried out to match data available from cerebral blood flow velocity, expired CO_2, and arterial pressure.

5.1. Eucapnia

5.1.1. Sensitivity analysis—For each of the cardiovascular and respiratory models, we computed and ranked relative sensitivities as described in Section 4.1.1. Results of this analysis (see Fig. 5) showed that both the cardiovascular and respiratory models contain sensitive and insensitive parameters, but that no clear break separates the two groups of parameters. Therefore, we separated parameters using an estimate based on the numerical integration accuracy. Numerical integration was done with accuracy 10^{-6}, and sensitivities were computed using finite difference Jacobians accurate to the order 10^{-3}. Thus, we included parameters with sensitivities greater than 10^{-3} in the subset selection analysis, while rejecting the remaining parameters. The model depends on both sensitive and insensitive parameters, thus the insensitive parameters cannot be taken out of the model. Instead, we kept these parameters fixed at their nominal parameter values. This cutoff choice allowed us to exclude the four valve parameters $x_{car,}insens = \{R_{tv,o}, R_{mv,o}, R_{av,o}, R_{pv,o}\}$ and 7 respiratory parameters $x_{resp,}insens = \{K_{O2}, k_{O2}, f_{v,tis}, V_{B,O2}, V_{T,O2}, f_{alv}\}$.

Note, for the respiratory model, the set of sensitive parameters did not include any parameters related to O_2. This is reasonable given that we had no measurements of partial pressure of O_2. In conclusion, parameters included in the set of sensitive parameters serve as candidates for subset selection as described in detail below.

5.1.2. Subset selection—For each model, we investigated correlations between parameters using subset selection as described in section 4.1.2. For the cardiovascular model, subset selection allowed us to extract six uncorrelated parameters from the set of sensitive parameters including $x_{car,sub} = \{R_B, R_S, C_{Sa}, T_M, f, E_{S,l}, E_{D,l}\}$. These results were obtained assuming that κ can be kept constant at its nominal parameter value. Including κ in subset selection result in a subset with κ instead of R_B (indicating that κ and R_B are correlated). However, since κ is a scaling factor, while R_B is the model parameter of interest, we chose to keep κ constant allowing identification of R_B. This observation is similar to results reported in previous studies [19, 24].

Nonlinear least squares estimation of the six cardiovascular parameters chosen by subset selection did not allow us to accurately reproduce the dynamics displayed by the data. An analysis of the remaining parameters (not picked by subset selection) revealed that including a seventh parameter, cerebral arterial compliance C_{Ba}, allowed us to better reproduce the dynamics displayed by the data. Since the objective is to analyze data from a patient with CHF it is reasonable that this parameter should be included. Also typical of CHF is an increased blood volume, which would induce an increased compliance in order to maintain a normal arterial pressure. Note that the systemic arterial compliance was already included in the subset, but that neither of the venous compliances were included. The latter may again be related to the fact that we have no data on the venous side. We remind the reader that subset selection was based on initial parameter values. Therefore, we repeated subset selection with the optimized parameter values, and at this stage C_{Ba} was included in the subset. Results from subset selection with the respiratory model revealed that we can identify 4 of the sensitive parameters including $x_{resp,sub} = \{V_D, M_{S,CO2}, M_{B,CO2}, V_{B,CO2}\}$.

Note, the CO_2 dissociation constants were set at literature values and thus not*[notdef]*included in the subset selection.

In summary, with subset selection we identified 11 parameters (7 cardiovascular and 4 respiratory) that can be estimated reliably given the data available for this study. This is a significant reduction from the total of 43 model parameters. However, it should be noted that model prediction does depend on the value of all 43 parameters, thus care must be taken to use realistic patient-specific physiological values for the parameters that are not included in the subset.

5.1.3. Parameter estimation—As described in Section 4.1 and shown on Fig. 3 nonlinear estimation was done in two steps. First we estimated the subset of parameters identified for the cardiovascular model, then we estimated the respiratory parameters. For both models, parameters were estimated using the Levenberg-Marquardt variant of the Gauss-Newton optimization method as described in Section 4.1.3. Optimized parameters are given in Table 1 for both the cardiovascular and respiratory models. All data were subsampled at 64 Hz to speed up computations and as discussed in Section 4.1 to allow the respiratory model to reach steady state, computations were done on a data-set repeated 40 times. Though the least squares error between computed and measured values of partial pressure of CO_2 was done only using the last repeat of the respiratory data as discussed. To verify that 40 repetitions of respiratory data was sufficient for achieving steady state, we compared results with those obtained with 60 and 80 repetitions. Parameter estimates with 40 repetitions varied less than 5% from those obtained with 80 repetitions, while the difference in estimates using 60 and 80 repetitions were less than 2%. Moreover, using 80 repetitions almost doubles the computation time, thus we decided that the 5% difference was acceptable. Results showing that with optimized parameters, our model is able to predict observed data are shown in Figs. 6 and 7. Note the model nicely predicts systolic and diastolic values, while the waveform is not reproduced exactly, this is due to the fact, that the circuit model used in this study does not account for wave-propagation, i.e., it is not able to predict the actual waveforms with an incoming and reflected wave. This can be seen from the large scale plots given in the right column of Fig. 9. Moreover, for ejection fraction EF, we only have one measurement given an overall ejection fraction of 26%. There will be variation over steady state, also shown in Fig. 9. On the other hand, respiratory data does not include major phenomena not accounted for by the model, thus the better fit to data as shown in Fig. 7.

5.2. Eucapnia followed by hypercapnia

Hypercapnia was induced by increasing inspired CO_2. To predict the effect of cerebral autoregulation, we used nonlinear optimization to estimate parameters representing the cerebral vascular resistance (R_B) under hypercapnic conditions. It should be noted that the cardiovascular model does not depend on the respiratory model, consequently parameters used for prediction of R_B were estimated using the cardiovascular model by minimizing the least squares error between computed and measured values of cerebral blood flow velocity v_{MCA}. The predicted time course of the cerebral vascular resistance is shown in Fig. 8, and the associated blood flow velocity in the middle cerebral artery is shown in the top left panel

of Fig. 9. Subsequently, we used the coupled model to estimate the subset of respiratory parameters identified during eucapnia. This was done by minimizing the least squares error between measured and computed values of expiratory CO_2 partial pressure. Results of this computation are shown in the remaining panels of Fig. 9. As for the steady state simulations, the model is able to predict the overall dynamics displayed by the data. Systolic and diastolic values were predicted accurately ($R^2 = 0.88$ and 0.84, respectively), with $R^2 = 0.72$ accounting for the entire waveform. The lower value is obtained because the model cannot predict secondary oscillations due to the lack of its ability to reflect wave propagation. Finally, respiratory dynamics were estimated accurately ($R^2 = 0.96$), reflecting that the model closely resembles dynamics observed in data.

6. Discussion

Results from the cardiovascular and respiratory models (Figs. 6 and 7) showed that the approach used in this study allowed prediction of cerebral CO_2 reactivity, via prediction of cerebral vascular resistance R_B, which can be directly related to cerebral vasodilation. Additionally, the models were able to predict observed data including cerebral blood flow velocity, arterial blood pressure, ejection fraction, and expiratory CO_2 partial pressure. Below we first discuss implications of the results obtained during eucapnia, and then we discuss results obtained during the transition from eucapnia to hypercapnia. We note that the subject studied was chosen since he displayed normal cerebral CO_2 reactivity and aside from CHF did not display other cardiovascular diseases.

Results from the cardiovascular and respiratory models (Figs. 6 and 7) showed that the approach used in this study allowed prediction of cerebral CO_2 reactivity, via prediction of cerebral vascular resistance R_B, which can be directly related to cerebral vasodilation. Additionally, the models were able to predict observed data including cerebral blood flow velocity, arterial blood pressure, ejection fraction, and expiratory CO_2 partial pressure. Below we first discuss implications of the results obtained during eucapnia, and then we discuss results obtained during the transition from eucapnia to hypercapnia. Finally, we note that the subject studied was chosen since he displayed normal cerebral CO_2 reactivity and aside from CHF did not display other cardiovascular diseases.

6.1. Eucapnia

During eucapnia, the cardiovascular model does not depend on any quantities computed by the respiratory model, while the respiratory model depends on blood flows predicted by the cardiovascular model. Since blood flow oscillate around a steady state during eucapnia and respiratory oscillations are significantly slower, it was sufficient to compute average blood flow values over the entire steady state interval and use these as inputs to the respiratory model. We checked results from the two step approach by computing the full dynamics using the coupled cardiovascular-respiratory model. We found that these predictions were indistinguishable from those obtained from sequential solution of the two models. A consequence of this observation is that accounting for pulsatile blood flow (as is done by the coupled model) does not significantly impact respiratory model dynamics.

In addition to computing model outcomes, we also computed all internal states and these were all within physiological bounds. This is important to verify because the nonlinear least squares optimization technique used for parameter estimation does not guarantee that internal states cannot deviate from physiological values, even if predicted values for the parameters optimized are within physiological bounds. Importantly, we compare internal states particular to CHF, characterized in this patient by a severely enlarged left ventricle and reduced ejection fraction at 26%. Optimized parameters revealed that the maximum left ventricular volume was approximately 411 ml and minimum ventricular volume was approximately 309 ml. These values yielding a stroke volume of 102 ml, with an average heart rate of 62.7 beats per minute, this gives an approximate CO of 6.4 L/min (see Appendix Table 3). This number corresponds to the cardiac output obtained from calculating the mean flow in the systemic or pulmonary circulations.

CHF implies reduced heart function however cardiac output can stay near normal levels in the early stages of CHF as the ventricle remodels and other controls work to keep cardiac output normal. In the end, these changes cause damage that reduces cardiac output (see presentation in [49]). For this patient, with left heart failure (but no sleep apnea) left ventricular end diastolic volume (LVEDV) is derived to be (double normal values but physiological for CHF patients without sleep apnea (left heart failure patients with sleep apnea have significantly larger LVEDV [50]). Given that the heart rate is normal and ejection fraction is 26% that implies such a very high LVEDV if cardiac output is to be normal. The fact that heart rate is normal and no other symptoms are present suggests a normal cardiac output (cardiac output data is not available). When cardiac output starts to reduce, as it will eventually in CHF, heart rate can possibly increase to compensate for a while. Thus in this patient it will likely take a very low ejection fraction to cause the kind of reduced cardiac output seen in CHF as the disease progresses.

Moreover, systemic venous pressure, pulmonary arterial pressure, and pulmonary venous pressure were approximately 3.6 mmHg, 27 mmHg, and 6.3 mmHg respectively, all with the range of expected values for a patient with CHF (see Table 2). The total resistance $R_{Tot} = (1/T_{BTot} + 1/R_S)-1 = 0.70$, where $R_{BTot} = R_{Ba} + R_B + R_{BV}$ is fairly low, but again expected for CHF. The low resistance may be an indicator of poor circulation in the lower extremities. Finally, we noted that during eucapnia approximately 25% of cardiac output was utilized as cerebral blood flow. This is a bit high, however, cerebral blood flow velocity measured for this subject was significantly larger than mean velocities reported in the literature [59]. This could be due to poor circulation in the lower body or exceptionally high values from the transcranial Doppler measurements. However, it could also be a result of the simplified modeling of the cerebral arteries. The blood flow velocity is measured in the middle cerebral arteries, and this has then been scaled (assuming constant area of the major cerebral arteries) to compute a total flow to the brain. Without information about anatomical quantities for the size of the cerebral arteries, this scaling factor is only as accurate as our estimates of patient anatomy. The magnitude of the scaling factor κ would impact the optimized values for the cerebral vascular resistance R_B since these two parameters are correlated as stated earlier. However, if the area of all major cerebral vessels (PCA, MCA and ACA) were measured, then this scaling parameter could be computed explicitly from the data.

For the respiratory quantities, values for dead space $p_{D,CO2}$ and $p_{D,O2}$, arterial values $p_{a,CO2}$ and $p_{a,O2}$, and systemic values $p_{S,CO2}$ and $p_{S,O2}$ (the latter calculated from concentrations and dissociation laws) are reasonable (compare [37, 38, 36]). Dead space values of CO_2 for normal inspired air oscillate between zero (inhaled air) and end-expiratory air approximately the same as alveolar air. Oxygen values follow similar reasonable patterns. It should be noted that brain partial pressures $p_{B,CO2}$ and $p_{B,O2}$ did not match typical values as well in the optimized case. The value for $p_{B,CO2}$ was approximately 44 mmHg (too low) and $p_{B,O2}$ approximately 50 mmHg (too high). There are likely several reasons for this. First, the data for cerebral blood velocity for this subject was higher than expected, which would tend to depress brain $p_{B,CO2}$ and raise $p_{B,O2}$. Second, we did not have data on O_2 which might impact the results. Further, research indicates that cerebral metabolism may be abnormal in patients with CHF, leading to possible metabolic imbalance [60]. In addition, given the complex effects induced by CHF in regards to the relation between heart rate and contractility [61] and the fact that the modeled CO_2 challenge induces only a 10% change in heart rate, we omitted a heart rate dependent change in contractility reflecting a Bowditch effect. The elastance parameters reflecting contractility were optimized for the steady state using subject specific data. We also recognize that the value estimated from literature for the FRC is only valid for individuals with no respiratory conditions, thus an extension of this model to CHF patients co-presenting with respiratory dysfunction would require a modified FRC estimate.

6.2. Eucapnia followed by hypercapnia

As discussed above, our model produced good predictions of behavior during eucapnia. In this section we discuss impact of the transition from eucapnia to hypercapnia. When the body is exposed to air with a high concentration of CO_2, it responds by activating control mechanisms to eliminate excess CO_2. The autonomic regulatory system increases heart rate and breathing depth and frequency while the cerebral autoregulatory system dilates vessels in the brain to allow faster washout of CO_2. The autonomic responses are incorporated in the model via model inputs, and thus, will not be discussed further here. Vasodilation enforced by cerebral autoregulation was modeled via dynamic regulation of cerebral vascular resistance. In physiological terms, the concentration of CO_2 should mediate changes in cerebral vascular resistance. As a first step towards elucidating the dynamics of this physiological connection, we used an empirical model predicting dynamics of cerebral vascular resistance directly by estimating nodes in a piecewise linear spline based on cerebral blood flow. This approach allowed prediction of cardiovascular dynamics independent of the respiratory model. Results showed the expected response behavior that cerebral vascular resistance decreased leading to an associated increase in cerebral blood flow velocity.

To ensure that the respiratory model was able to accurately predict expiratory CO_2 partial pressure, a final simulation was performed re-estimating the subset of respiratory parameters. This simulation did not move respiratory parameters significantly, since the majority of the dynamics were already identified during the steady state simulation.

Another detail which could improve patient-specific results involves adjusting the integration constant arising in (17) which is currently taken as the functional residual capacity (FRC) [ml] (as estimated as a function of height h [cm] and weight w [kg] [25]). This integration constant could be increased to reflect a higher *effective* basic CO_2 volume due to its higher ability to diffuse into tissues compared to O_2 (see e.g. [38]). Since we were estimating FRC from a general formula we did not include such a correction. When fitting the data to specific patients one could seek to acquire more information to adjust the integration constant to reflect this.

In future work, we plan to incorporate a model predicting $R_B(c_{B,CO2},t)$, that is, changes in R_B dependent on cerebral CO_2 level. The current model provides a way to estimate cerebral CO_2 via a model and parameter estimation from data for measured expired CO_2. At this point, R_B is estimated from cerebral blood flow velocity. The link will be complete once a model that connects R_B and cerebral CO_2 is developed. Once this is done, it will be possible to estimate cerebral CO_2 reactivity using non-invasive measurements from CO_2 breathing tests.

7. Conclusion

The results discussed here indicate that the proposed methodology and model can be used for numerically efficient estimation of parameters for any subject with CHF and hence can be also used for quantitatively studying variations between subjects with CHF and subjects who suffer from CHF and central sleep apnea [3, 2, 4, 1], periodic breathing [62, 63], compromised breathing stability [64], greater central and peripheral reactivity to CO_2 [65, 66], and attenuated cerebral vascular reactivity resulting from brain hypoperfusion [66, 67, 68, 6]. Understanding how the control systems are compromised has potential to provide more insight into these diseases. Future studies could include an extension of the proposed method to a cohort of similar patients, to both analyze differences in parameter values across the group at a particular time point and understand the progression of disease progression in time. However, to use this model to compare quantities from a larger population it should be emphasized that the model should be used with care. First, a physiology-based model as a function of tissue CO_2 could improve prediction of cerebral vascular resistance dynamics. One could also expand the complexity of the interactions influencing the dynamics affecting expiratory CO_2. Second, more effort could be put into developing faster methods for parameter estimation.

Moreover, it is important that nominal parameters reflect known characteristics from a subject with CHF, in particular since only a subset of the parameters will be estimated. Therefore, conclusions based on analysis of parameters obtained from several subjects should all be interpreted related to the nominal parameter values used. Furthermore, additional measurements would increase predictability of the model parameters, in particular it would be beneficial to include measurements of cardiac output and estimation of diameters of major cerebral vessels. Knowing these quantities would allow better prediction of systemic and arterial flow as well as help to get better estimation of the scaling factor needed, which would help in prediction of the scaling factor relating flow and velocity in the middle cerebral artery. Finally, it should be noted that parameter estimates predicted here are

found using a local method. Thus, there is no guarantee that the predicted values are truly optimal. However, since nominal values were assumed close to the physiological values for the specific subject, estimated values are physiologically relevant. Another use of the subset selection methods applied here, is for model reduction. If the model output is insensitive to a given group of parameters it may be possible to use this information to reduce the model.

Finally, we mention that the analysis of the correlation between parameters using the above methods might potentially suggest new links between systems and hence suggest new physiological information as long as the correlation is not introduced simply as a consequence of the model reduction or model structure.

Acknowledgments

Olufsen was partially supported by National Science Foundation under Grants DMS-1022688, DMS-0616597, and OISE-524249 (the latter two grants also supported Ellwein while at NCSU) and National Institute of Health under Grant 1P50 GM094503-01A1, Batzel was supported in part by FWF (Austrian Research Funds) Project P18778-N13, Pope and Kelley were supported in part by National Science Foundation under Grants DMS-0707220 and CDI-0941253 and by the Army Research Office under Grant W911NF-11-1-0367, and Xie was supported in part by the American Lung Association of Wisconsin.

Appendix

A.1. Cardiovascular model

The following give equations for blood pressures and ventricular volumes. The main symbols are *p*, *V*, and *C* for pressure, volume, and compliance, respectively. Subscript symbols *P*, *S*, and *B* denote pulmonary, systemic, and brain regions, respectively. Subscripts *a* and v in vascular pressure equations denote generally arterial and venous, respectively, except for the resistances entering and leaving the heart. In that case R_{mv}, R_{tv}, R_{av}, and R_{pv} denote mitral valve, tricuspid valve, aortic valve, and pulmonary valve resistances while *lv* and *rv* denote left and right ventricle, respectively, in the ventricular equations.

Blood pressures, ventricular volumes, and intrathoracic pressure

$$\begin{aligned}
\frac{dp_{Pa}}{dt} &= \left(\frac{p_{rv}-p_{Pa}}{R_{pv}} - \frac{p_{Pa}-p_{Pv}}{R_P}\right)/C_{Pa}\\
\frac{dp_{Pv}}{dt} &= \left(\frac{p_{Pa}-p_{Pv}}{R_P} - \frac{p_{Pv}-p_{lv}}{R_{mv}}\right)/C_{Pv}\\
\frac{dp_{Sa}}{dt} &= \left(\frac{p_{lv}-p_{Sa}}{R_{av}} - \frac{p_{Sa}-p_{Sv}}{R_S} - \frac{p_{Sa}-p_{Ba}}{R_{Ba}}\right)/C_{Sa}\\
\frac{dp_{Sv}}{dt} &= \left(\frac{p_{Sa}-p_{Sv}}{R_S} + \frac{p_{Bv}-p_{Sv}}{R_{Bv}} - \frac{p_{Sv}-p_{rv}}{R_{tv}}\right)/C_{Sv}\\
\frac{dp_{Ba}}{dt} &= \left(\frac{p_{Sa}-p_{Ba}}{R_{Ba}} - \frac{p_{Ba}-p_{Bv}}{R_B}\right)/C_{Ba}\\
\frac{dp_{Bv}}{dt} &= \left(\frac{p_{Ba}-p_{Bv}}{R_B} - \frac{p_{Bv}-p_{Sv}}{R_{Bv}}\right)/C_{Bv}\\
\frac{dV_{lv}}{dt} &= \frac{p_{Pv}-p_{lv}}{R_{mv}} - \frac{p_{lv}-p_{Sa}}{R_{av}}\\
\frac{dV_{rv}}{dt} &= \frac{p_{Sv}-p_{rv}}{R_{tv}} - \frac{p_{rv}-p_{Pa}}{R_{pv}}
\end{aligned} \tag{27}$$

Heart valves

$$\begin{aligned} R_{av} &= \min\left[R_{av,o}+e^{-2\left(p_{lv}-p_{Sa}\right)}, R_{av,c}\right] \\ R_{mv} &= \min\left[R_{mv,o}+e^{-2\left(p_{Pv}-p_{lv}\right)}, R_{mv,c}\right] \\ R_{pv} &= \min\left[R_{pv,o}+e^{-2\left(p_{rv}-p_{Pa}\right)}, R_{pv,c}\right] \\ R_{tv} &= \min\left[R_{tv,o}+e^{-2\left(p_{Sv}-p_{rv}\right)}, R_{tv,c}\right] \end{aligned}$$

Ventricular pressures

$$\begin{aligned} p_{lv}(t) &= E_{lv}(t)\left[V_{lv}(t)-V_{ld}\right] \\ p_{rv}(t) &= E_{rv}(t)\left[V_{rv}(t)-V_{rd}\right] \end{aligned}$$

where

$$E_{lv}(t) = \begin{cases} E_{D,l}+\left(E_{S,l}-E_{D,l}\right)\left[1-cos\left(\frac{\pi t}{T_M}\right)\right]/2 & 0 \le t \le T_M \\ E_{D,l}+\left(E_{S,l}-E_{D,l}\right)\left[cos\left(\frac{\pi\left(t-T_M\right)}{T_R}\right)+1\right]/2 & T_M \le t \le T_M+T_R \\ E_{D,l} & T_M+T_R \le t \le T, \end{cases}$$

$$E_{rv}(t) = \begin{cases} E_{D,r}+\left(E_{S,r}-E_{D,r}\right)\left[1-cos\left(\frac{\pi t}{T_M}\right)\right]/2 & 0 \le t \le T_M \\ E_{D,r}+\left(E_{S,r}-E_{D,r}\right)\left[cos\left(\frac{\pi\left(t-T_M\right)}{T_R}\right)+1\right]/2 & T_M \le t \le T_M+T_R \\ E_{D,r} & T_M+T_R \le t \le T \end{cases}$$

Note, the timing parameters T_M and T_R are the same for both the left and right ventricles. Input to this model is heart rate H. Outcomes from the model is arterial blood pressure $p_{Sa}(t)$, cerebral blood flow velocity $v_{\mathrm{MCA}} = q_B/k$, and ejection fraction EF. Initial values for the differential equations as well as nominal and optimal parameter values are listed in the Appendix, Table 3.

A.2. Respiratory model

The following give equations for partial pressures and concentrations in the respiratory system. The main symbols are p and c for partial pressure and concentration. Subscript symbols S and B refer to the systemic arteries and the brain, subscripts CO_2 and O_2 refer to the two main gases. Metabolic rates are denoted by M and diffusion coefficients by D. Finally, the respiratory model depends on flows q_i predicted by the cardiovascular model.

Systemic tissue

$$\begin{aligned}
\frac{dc_{Stis,CO_2}}{dt} &= \left(M_{S,CO_2} - D_{S,CO_2}\left(c_{Stis,CO_2} - c_{Scap,CO_2}\right)\right)/V_{Stis,CO_2} \\
\frac{dc_{Scap,CO_2}}{dt} &= \left(q_S\left(c_{a,CO_2} - c_{Scap,CO_2}\right) + D_{S,CO_2}\left(c_{Stis,CO_2} - c_{Scap,CO_2}\right)\right)/V_{Scap,CO_2} \\
\frac{dc_{Stis,O_2}}{dt} &= \left(M_{S,O_2} - D_{S,O_2}\left(c_{Stis,O_2} - c_{Scap,O_2}\right)\right)/V_{Stis,O_2} \\
\frac{dc_{Scap,O_2}}{dt} &= \left(q_S\left(c_{a,O_2} - c_{Scap,O_2}\right) + D_{S,O_2}\left(c_{Stis,O_2} - c_{Scap,O_2}\right)\right)/V_{Scap,O_2}
\end{aligned}$$

Brain tissue

$$\begin{aligned}
\frac{dc_{Btis,CO_2}}{dt} &= \left(M_{B,CO_2} - D_{B,CO_2}\left(c_{Btis,CO_2} - c_{Bcap,CO_2}\right)\right)/V_{Btis,CO_2} \\
\frac{dc_{Bcap,CO_2}}{dt} &= \left(q_{Bv}\left(c_{a,CO_2} - c_{Bcap,CO_2}\right) + D_{B,CO_2}\left(c_{Btis,CO_2} - c_{Bcap,CO_2}\right)\right)/V_{Bcap,CO_2} \\
\frac{dc_{Btis,O_2}}{dt} &= \left(M_{B,O_2} - D_{B,O_2}\left(c_{Btis,O_2} - c_{Bcap,O_2}\right)\right)/V_{Btis,O_2} \\
\frac{dc_{Bcap,O_2}}{dt} &= \left(q_{Bv}\left(c_{a,O_2} - c_{Bcap,O_2}\right) + D_{B,O_2}\left(c_{Btis,O_2} - c_{Bcap,O_2}\right)\right)/V_{Bcap,O_2}
\end{aligned}$$

In the above equations, D_T is the diffusion capacity for a gas, $V_{Ttis,g}$ is the effective tissue volume for a gas, $V_T cap$ is the effective systemic capillary blood volume for blood flow through a tissue for a gas (approximately 1% of V_T).

Inspiration

$$\begin{aligned}
\frac{dp_{D1,CO_2}}{dt} &= \dot{V}_{ie}\left(p_{I,CO_2} - p_{D1,CO_2}\right)/V_{D1} \\
\frac{dp_{D1,O_2}}{dt} &= \dot{V}_{ie}\left(p_{I,O_2} - p_{D1,O_2}\right)/V_{D1} \\
\frac{dp_{D2,CO_2}}{dt} &= \dot{V}_{ie}\left(p_{D1,CO_2} - p_{D2,CO_2}\right)/V_{D2} \\
\frac{dp_{D2,O_2}}{dt} &= \dot{V}_{ie}\left(p_{D1,O_2} - p_{D2,O_2}\right)/V_{D2} \\
\frac{dp_{D3,CO_2}}{dt} &= \dot{V}_{ie}\left(p_{D1,CO_2} - p_{D3,CO_2}\right)/V_{D3} \\
\frac{dp_{D3,O_2}}{dt} &= \dot{V}_{ie}\left(p_{D1,O_2} - p_{D3,O_2}\right)/V_{D3} \\
\frac{dp_{a,CO_2}}{dt} &= 863 \cdot 0.98 \cdot q_P\left(c_{v,CO_2} - c_{a,CO_2}\right) + \dot{V}_{ie}\left(p_{D3,CO_2} - p_{a,CO_2}\right)/V_A \\
\frac{dp_{a,O_2}}{dt} &= 863 \cdot 0.98 \cdot q_P\left(c_{v,O_2} - c_{a,O_2}\right) + \dot{V}_{ie}\left(p_{D3,O_2} - p_{a,O_2}\right)/V_A
\end{aligned}$$

Expiration

$$
\begin{aligned}
\frac{dp_{D1,CO_2}}{dt} &= \dot{V}_{ie}\left(p_{D1,CO_2} - p_{D2,CO_2}\right)/V_{D1} \\
\frac{dp_{D1,O_2}}{dt} &= \dot{V}_{ie}\left(p_{D1,O_2} - p_{D2,O_2}\right)/V_{D1} \\
\frac{dp_{D2,CO_2}}{dt} &= \dot{V}_{ie}\left(p_{D2,CO_2} - p_{D3,CO_2}\right)/V_{D3} \\
\frac{dp_{D2,O_2}}{dt} &= \dot{V}_{ie}\left(p_{D2,O_2} - p_{D3,O_2}\right)/V_{D2} \\
\frac{dp_{D3,CO_2}}{dt} &= \dot{V}_{ie}\left(p_{D3,CO_2} - p_{a,CO_2}\right)/V_{D3} \\
\frac{dp_{D3,O_2}}{dt} &= \dot{V}_{ie}\left(p_{D3,O_2} - p_{a,O_2}\right)/V_{D3} \\
\frac{dp_{a,CO_2}}{dt} &= 863 \cdot 0.98 \cdot q_P\left(c_{v,CO_2} - c_{a,CO_2}\right)/V_A \\
\frac{dp_{a,O_2}}{dt} &= 863 \cdot 0.98 \cdot q_P\left(c_{v,O_2} - c_{a,O_2}\right)/V_A
\end{aligned}
$$

Note, instantaneous airflow is obtained from integrating the air flow velocity data as described in equation (17). Inputs to the respiratory model include airflow velocity, average systemic, pulmonary, and cerebral blood flow obtained by solving the cardiovascular model. For the coupled model, these flows are computed at any instant in time. Initial values, and nominal and optimized parameter values for the respiratory model are given in the Appendix, Table 4.

References

1. Batzel J, Kappel F, Timischl-Teschl S. A cardiovascular-respiratory control system model including state delay with application to congestive heart failure in humans. J Math Biol. 2005; 50:293–335. [PubMed: 15480669]
2. Cherniack N. Apnea and periodic breathing during sleep. New England J Med. 1999; 341:985–987. [PubMed: 10498496]
3. Garcia-Touchard A, Somers V, Olson L, Caples S. Central sleep apnea: implications for congestive heart failure. Chest. 2008; 133:1495–1504. [PubMed: 18574295]
4. Longobardo G, Cherniack N, Gothe B. Factors affecting respiratory system stability. Ann Biomed Eng. 1989; 17:377–396. [PubMed: 2774313]
5. Morgan B, Reichmuth K, Peppard P, Finn L, Barczi S, Young T, Nieto F. Effects of sleep disordered breathing on cerebrovascular regulation: A population based study. Am J Resp Crit Care Med. 2010; 182:1445–1452. [PubMed: 20639438]
6. Xie A, Skatrud J, Khayat R, Dempsey J, Morgan B, Russell D. Cerebrovascular response to carbon dioxide in patients with congestive heart failure. Am J Resp Crit Care Med. 2005; 172:371–378. [PubMed: 15901613]
7. Dong F, Langford W. Models of cheyne-stokes respiration with cardiovascular pathologies. J Math Biol. 2008; 57:497–519. [PubMed: 18392825]
8. Lu K, Clark J, Ghorbel F, Ware D, Bidani A. A human cardiopulmonary system model applied to the analysis of the valsalva maneuver. Am J Physiol. 2001; 281:H2661–H2679.
9. Lu K, Clark W, Ghorbel F, Robertson C, Ware D, Zwischenberger J, Bidani A. Cerebral autoregulation and gas exchange studied using a human cardiopulmonary model. Am J Physiol. 2004; 286:H584–H601.
10. Ainslie PN, Ashmead J, Ide K, Morgan B, Poulin MJ. Differential responses to co_2 and sympathetic stimulation in the cerebral and femoral circulations in humans. J Physiol. 2005; 566:613–624. [PubMed: 15890697]

11. Ainslie PN, Duffin J. Integration of cerebrovascular co2 reactivity and chemoreflex control of breathing: mechanisms of regulation, measurement, and interpretation. Am J Physiol. 2009; 296:R1473–R1495.
12. Ottesen, JT.; Olufsen, MS.; Larsen, J. Applied Mathematical Models in Human Physiology. SIAM; Philadelphia, PA: 2004.
13. Rideout, V. Mathematical and Computer Modeling of Physiological Systems. Prentice Hall; Englewood Cliffs, NJ: 1991.
14. Stergiopoulos N, Meister J, Westerhof N. Determinants of stroke volume and systolic and diastolic aortic pressure. Am J Physiol. 1996; 270:H2050–H2059. [PubMed: 8764256]
15. Ursino M. Interaction between carotid baroregulation and the pulsating heart: a mathematical model. Am J Physiol. 1998; 44:H1733–H1747. [PubMed: 9815081]
16. Schroff G, Janicki J, Weber K. Left ventricular systolic dynamics in terms of its chamber mechanical properties. Am J Physiol. 1983; 14:H110–H124.
17. Olufsen M, Ottesen J, Tran H, Ellwein L, Lipsitz L, Novak V. Blood pressure and blood flow variation during postural change from sitting to standing: model development and validation. J Appl Physiol. 2005; 99:1523–1537. [PubMed: 15860687]
18. Ellwein L, Tran H, Zapata C, Novak V, Olufsen M. Sensitivity analysis and model assessment: mathematical models for arterial blood flow and blood pressure. J Cardiovasc Eng. 2008; 8:94–108.
19. Pope S, Ellwein L, Zapata C, Novak V, Kelley C, Olufsen M. Estimation and identification of parameters in a lumped cerebrovascular model. Math Biosci Eng. 2009; 6:93–115. [PubMed: 19292510]
20. Chen X, Qi L, Teo K-L. Smooth convex approximation to the maximum eigenvalue function. J Global Opt. 2004; 30:253–270.
21. Conrad S, Brown E, Grier L, Baier J, Blount J, Heming T, Zwischenberger J, Bidani A. Arteriovenous extracorporeal carbon dioxide removal a mathematical model and experimental evaluation. ASAIO Journal. 1998; 44:267–277. [PubMed: 9682952]
22. Berne, R.; Levy, M. Physiology. 2nd Edition. C.V. Mosby Company; St Louis, MO: 1988.
23. Boron, W.; Boulpae, E. Medical Physiology. W. B. Saunder; 2003.
24. Ellwein, L. Ph.D. thesis. Dept Mathematics, North Carolina State University; Raleigh, NC: 2008. Cardiovascular and respiratory regulation, modeling and parameter estimation.
25. Stocks J, Quanjer P. Reference values for residual volume, functional residual capacity and total lung capacity. J Biomech Eng. 2002; 124:9–20. [PubMed: 11871610]
26. Guyton, A.; Hall, J. Textbook of Medical Physiology. W. B. Saunders; Philadelphia, PA: 1996.
27. Tkacova R, Hall M, Liu P, Fitzgerald F, Bradley T. Left ventricular volume in patients with heart failure and cheyne-stokes respiration during sleep. Am J Respir Crit Care Med. 1997; 156:1549–1555. [PubMed: 9372674]
28. Ottesen J, Danielsen M. Modeling ventricular contraction with heart rate changes. J Theo Biol. 2003; 22:337–346.
29. Heldt, T. Computational models of cardiovascular response to orthostatic stress, Ph.D. thesis. Harvard/MIT Division of Health Science and Technology; Cambridge, MA: 2004.
30. Baker R, Kozoll D, Meyer K. The use of surface area as a basis for establishing normal blood volume. Surg Gynecol Obstet. 1957; 104:183–189. [PubMed: 13422132]
31. Mosteller R. Simplified calculation of body surface area. N Engl J Med. 1987; 317:1098. [PubMed: 3657876]
32. Beneken, J.; DeWitt, B. A physical approach to hemodynamic aspects of the human cardiovascular system. In: Reeve, E.; Guyton, A., editors. Physical Bases of Circulatory Transport: Regulation and Exchange. W. B. Saunders; Philadelphia, PA: 1967. p. 1-45.
33. DeVault K, Gremaud P, Olufsen VNV,M, Vernieres G, Zhao P. Blood flow in the circle of willis: Modeling and calibration. Multiscale Mod Simul: SIAM Int J. 2008; 7:888–909.
34. West G, Brown J, Enquist B. A general model for the origin of allometric scaling laws in biology. Science. 1997; 276:122–126. [PubMed: 9082983]

35. White C, Seymour R. Allometric scaling of mammalian metabolism. J Exp Biol. 2008; 208:1611–1619. [PubMed: 15855392]
36. Khoo M, Gottschalk A, Pack A. Sleep-induced periodic breathing and apnea: A theoretical study. J Appl Physiol. 1991; 70:2014–2024. [PubMed: 1907602]
37. Grodins FS, Buell J, Bart AJ. Mathematical analysis and digital simulation of the respiratory control system. J Appl Physiol. 1967; 22:260–276. [PubMed: 6017893]
38. Khoo M. A model-based evaluation of the single breath co_2 test. J Appl Physiol. 1990; 68:393–399. [PubMed: 2107168]
39. Thomas V, Costes F, Busso T. Estimation of arterial pco_2 from a lung model during ramp exercise in healthy young subjects. Resp Physiol Neurobiol. 2007; 156:259–265.
40. Fox, S. Human Physiology. 4th Edition. Wm. C. Brown Publishers; Dubuque, IA: 1993.
41. Otis, S.; Ringelstein, E. The transcranial doppler examination: principles and applications of transcranial doppler sonography. In: Tegeler, C.; Babikian, V.; Gomez, C., editors. Neurosonology. Mosby; St. Louis, MO: 1996. p. 140-155.
42. Farhi L, Rahn H. Dynamics of changes in carbon dioxide stores. Anesthesiology. 1960; 21:604–614. [PubMed: 13698175]
43. Miao H, Xia X, Perelson A, Wu H. On identifiability of nonlinear ode models and applications in viral dynamics. SIAM Review. 2011; 53:3–39. [PubMed: 21785515]
44. Olufsen M, Ottesen J. A practical approach to parameter estimation applied to model predicting heart rate regulation. J Math Biol. 2012:1–30. DOI:10.1007/s00285-012-0535-8.
45. Pope, S. Ph.D. thesis. Dept Mathematics, North Carolina State University; Raleigh, NC: 2009. Parameter identification in lumped compartment cardiorespiratory models.
46. Ipsen I, Kelley C, Pope S. Rank-deficient nonlinear least squares problems and subset selection. SIAM J Numer Anal. 2011; 49:1244–1266.
47. Dochain, D.; Vanrollegehem, P. Dynamical Modelling and Estimation in Wastewater Treatment Processes. IWA Publishing; Padstow, Cornwall, UK: 2001.
48. Kelley, C. Iterative Methods for Optimization. SIAM; Philadelphia, PA: 1999.
49. Mudd J, Kass D. Tackling heart failure in the twenty-first century. Nature. 2008; 451:919–928. [PubMed: 18288181]
50. Tkacova R, Hall M, Liu P, Fitzgerald F, Bradley T. Left ventricular volume in patients with heart failure and cheyne-stokes respiration during sleep. Am J Respir Crit Care Med. 1997; 156:1549–55. [PubMed: 9372674]
51. O'Dell K, Kalus J, Kucukarslan S, Czerska B. Nesiritide for secondary pulmonary hypertension in patients with end-stage heart failure. Am J Health Syst Pharm. 2005; 62:606–609. [PubMed: 15757881]
52. Magder S, Veerassamy S, Bates J. A further analysis of why pulmonary venous pressure rises after the onset of lv dysfunction. J Appl Physiol. Oct 9th. online first.
53. Katz AM. Heart failure: a hemodynamic disorder complicated by mal-adaptive proliferative responses. J Cell Mol Med. 2003; 7:1–10. [PubMed: 12767256]
54. Parmley W. Pathophysiology of congestive heart failure. Clin Cardiol. 1992; 15(Suppl):I5–I12. [PubMed: 1395215]
55. Mak S, Azevedo E, Liu P, Newton G. Effect of hyperoxia on left ventricular function and filling pressures in patients with and without congestive heart failure. Chest. 2001; 120:467–473. [PubMed: 11502645]
56. Chatterjee K, Massie B. Systolic and diastolic heart failure: differences and similarities. J Card Fail. 2007; 13:569–576. [PubMed: 17826648]
57. Fukuda N, Shinohara H, Sakabe K, Morishita S, Fukuda Y, Tamura Y. Evaluation of right ventricular function in patients with congestive left heart failure by the doppler derived total cardiac performance index (tei index). J Echocard. 2007; 5:11–17.
58. Francis G. Pathophysiology of chronic heart failure. Am J Med. 2001; 110:37S–46S. [PubMed: 11334774]

59. Gruhn N, Larsen F, Boesgaard S, Knudsen G, Mortensen S, Thomsen G, Aldershvile J. Cerebral blood flow in patients with chronic heart failure before and after heart transplantation. Stroke. 2001; 32:2530–2533. [PubMed: 11692012]
60. Lee C, Lee J, Kim J, Park S, Hong M, Kim S, Lim T, Park S. Cerebral metabolic abnormalities in congestive heart failure detected by proton magnetic resonance spectroscopy. J Am Coll Cardiol. 1999; 33:1196–1202. [PubMed: 10193716]
61. Petretta M, Vicario M, Spinelli L, Ferro A, Cuocolo A, Condorelli M, Bonaduce D. Combined effect of the forcefrequency and lengthtension mechanisms on left ventricular function in patients with dilated cardiomyopathy. Eur J Heart Fail. 2005; 4:727–735. [PubMed: 12453543]
62. Javaheri S, Parker TJ, Liming J, Corbett W, Nishiyama H, Wexler L, Roselle G. Sleep apnea in 81 ambulatory male patients with stable heart failure. types and their prevalences, consequences, and presentations. Circulation. 1998; 97:2154–2159. [PubMed: 9626176]
63. Sin D, Fitzgerald F, Parker J, Newton G, Floras J, Bradley T. Risk factors for central and obstructive sleep apnea in 450 men and women with congestive heart failure. Am J Respir Crit Care Med. 1999; 160:1077–1078. [PubMed: 10508791]
64. Xie A, Skatrud JV, Morgan B, Chenuel B, Khayat R, Reichmuth K, Lin J, Dempsey J. Influence of cerebrovascular function on the hypercapnic ventilatory response in healthy humans. J Physiol. 2006; 577(Pt 1):319–29. [PubMed: 16931556]
65. Solin P, Roebuck T, Johns DP, Walters E, Naughton M. Peripheral and central ventilatory responses in central sleep apnea with and without congestive heart failure. Am J Respir Crit Care Med. 2000; 162:2194–2200. [PubMed: 11112137]
66. Caparas S, Clair M, Krombach R, Hendrick J, Houck W, Kribbs S, Mukherjee R, Tempel G, Spinale F. Brain blood flow patterns after the development of congestive heart failure: effects of treadmill exercise. Crit Care Med. 2000; 28:209–214. [PubMed: 10667524]
67. Lee CW, Lee J, Lim T, Yang H, Hong M, Song J, Park S, Park S, Kim J. Prognostic significance of cerebral metabolic abnormalities in patients with congestive heart failure. Circulation. 2001; 103:2784–2787. [PubMed: 11401932]
68. Georgiadis D, Sievert M, Cencetti S. Cerebrovascular reactivity is impaired in patients with cardiac failure. Eur Heart J. 2000; 21:407–413. [PubMed: 10666355]

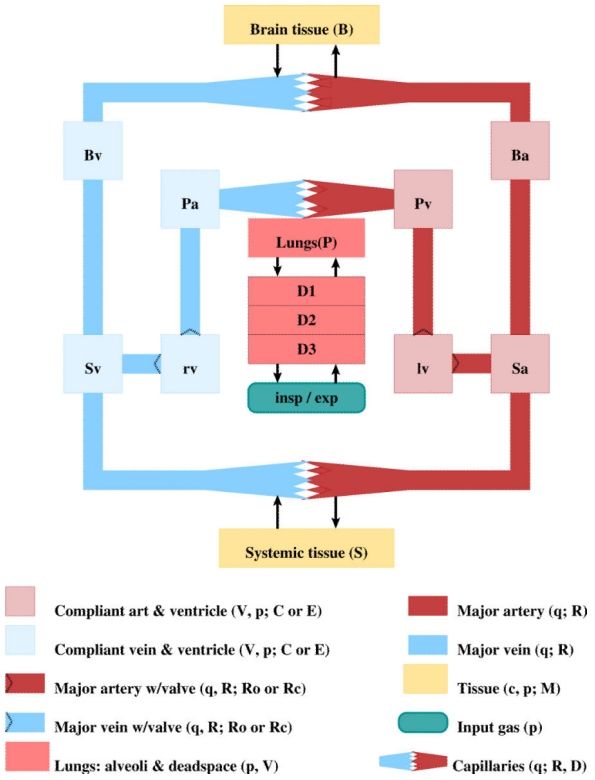

Figure 1.

Compartmental model of the cardiovascular and respiratory circulations. Systemic (subscript *S*), brain (subscript *B*), and pulmonary (subscript *P*) arteries (subscript *a*) and veins (subscript *v*); Vessels carrying oxygenated blood (systemic arteries and pulmonary veins) are red, while vessels carrying deoxygenated blood (systemic veins and pulmonary arteries) are blue. All vascular compartments represent a group of vessels with similar pressure p [mmHg]. Each vascular compartment is characterized by its volume V [ml] and compliance C [ml/mmHg]. The left (red, subscript lv) and right (blue, subscript rv) ventricles generate pulsatile pressure p_{lv}, p_{rv} [mmHg]. These two compartments are defined using time-varying elastance E [mmHg/ml]. Flow q [ml/s] between compartments are opposed by constant resistances [mmHg s/ml]. Gases diffuse from major arteries into the capillaries at a rate D. Tissue compartments (yellow) account for exchange of gases (O_2 and CO_2) with capillaries. Each vascular bed is characterized by a metabolic rate M [ml_{stpd}/s], and the gas concentrations in the tissues and capillaries are denoted by c [ml_{stpd}/ml]. The lungs are represented by three dead space compartments each predicting the partial pressure of the gases $p_{Di,g}$ [mmHg]. The partial pressure of the gases in the inspired air $p_{I,g}$, and the CO_2 expiratory partial pressure $p_{exp,CO2}$ are marked separately.

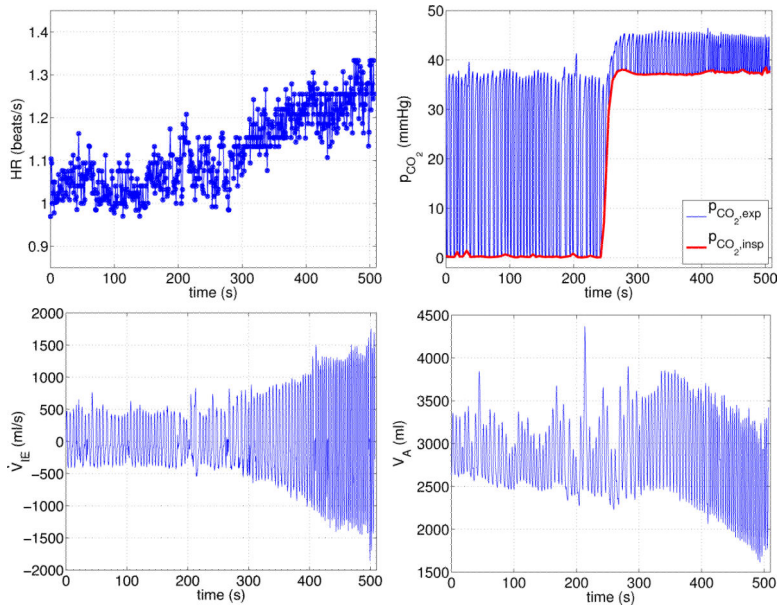

Figure 2.

Input to the model from experimental data. Top row: Heart rate (left panel) and inspired partial pressure of CO_2 (marked with a red line on the right panel). These values are obtained by fitting a smooth spline through minimum values of expiratory CO_2 partial pressures. Bottom row: Inspired airflow (left panel) and alveolar volume (right panel).

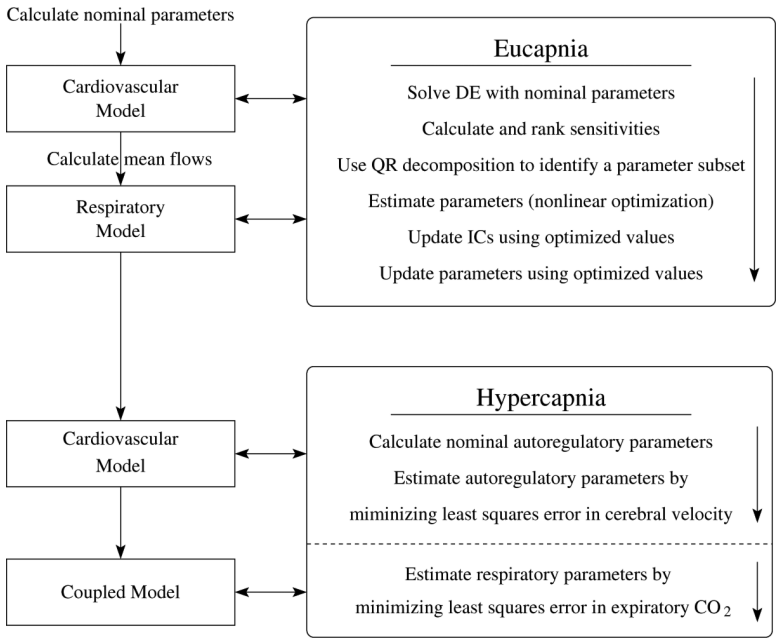

Figure 3.
Model analysis flow chart.

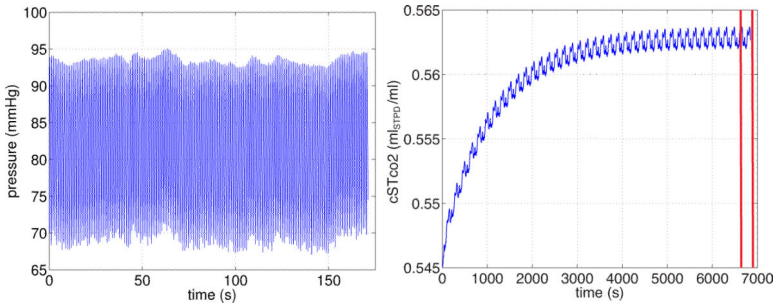

Figure 4.

Dynamics of arterial blood pressure p_{Sa} (left) and tissue concentration of CO_2 (right) during Eucapnia. Note, the cardiovasculatory model settles at steady state oscillations within the first 10 seconds, while the respiratory model takes more than an hour to equilibrate.

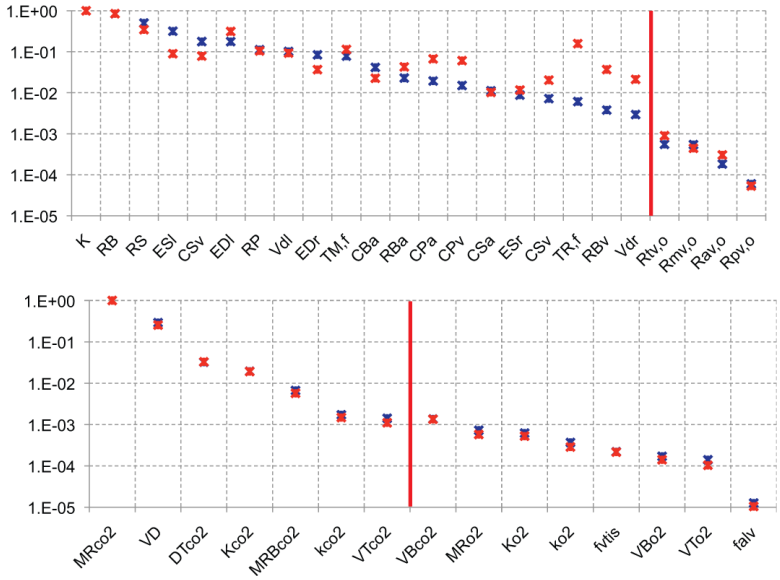

Figure 5.

Ranked sensitivities for the cardiovascular and respiratory models. The top graph shows ranking for the cardiovascular model and bottom graph shows ranking for the respiratory model. For both graphs, blue stars denote sensitivities computed using the initial (nominal) parameter values, and the red stars denote sensitivities computed using the optimized parameters. Note, that the y-axis is a log scale.

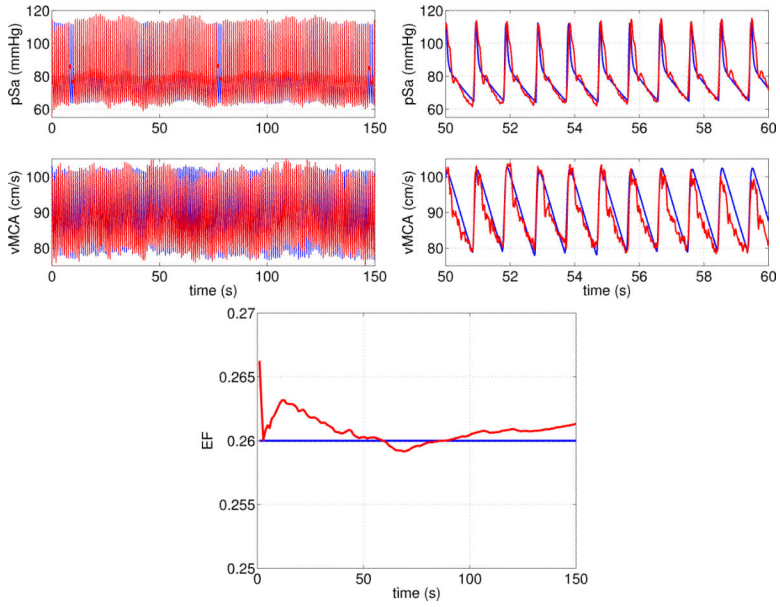

Figure 6.

Steady state simulation results from the cardiovascular model. Graphs show arterial pressure and cerebral blood flow velocity for the full dataset, and a zoom for $50 \leq t \leq 60$ seconds. The bottom panel shows computed and expected ejection fraction EF (set at 26%).

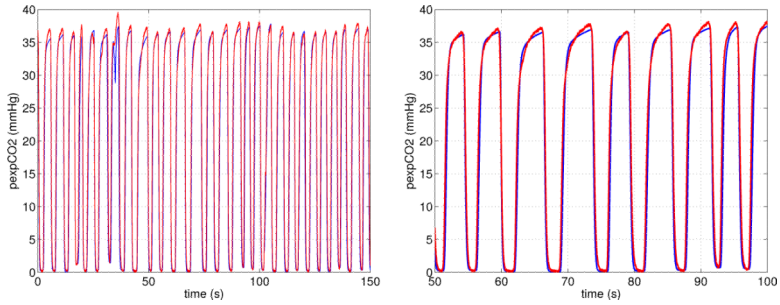

Figure 7.

Steady state simulation results from the respiratory model. The graphs show expiratory CO_2 partial pressure as a function of time. The left graph shows results over the complete time-series, while the right graph show a zoom for $50 \leq t \leq 100$ seconds.

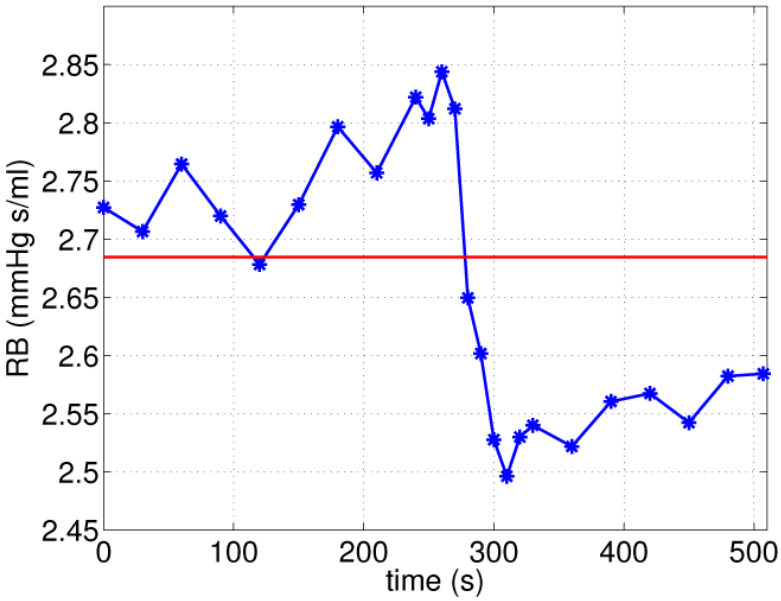

Figure 8.

Autoregulation of cerebral vascular resistance R_B. The red horizontal line shows the value obtained during eucapnia, while the time-varying blue line shows dynamics obtained during hypercapnia.

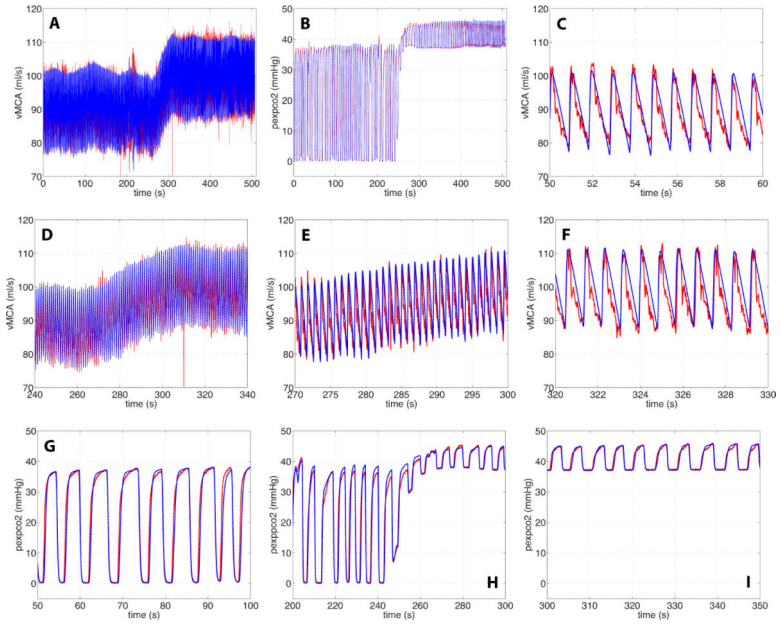

Figure 9.

Simulation results from the coupled model with controls. Panels A and B show the entire time-series predicting cerebral blood flow velocity and expiratory CO_2 partial pressure. Panels C-F show zoomed snapshots of cerebral blood flow velocity during normal breathing C, during the transition D and E, and during hypercapnia F. Panels G-I show zoomed snapshots of expiratory CO_2. G shows dynamics during normal breathing, H during the transition, I during hypercapnia. For all graphs the blue line denotes computed results, while the red line mark the associated experimental data.

Table 1

Nominal and optimal parameter values for the cardiovascular model (top) and the respiratory model (bottom).

Parameter	Physiologic description	Nominal value	Optimal value
$T_{M,f}$	Time to end-systole	0.35	0.137
$E_{D,r}$ [mmHg/ml]	Right ventricular diastolic elastance	0.0667	0.0167
$E_{S,l}$ [mmHg/ml]	Left ventricular systemic elastance	0.849	0.507
R_S [mmHg s/ml]	Systemic resistance	1.08	0.934
R_B [mmHg s/ml]	Cerebral resistance	4.25	2.69
C_{Sa} [ml/mmHg]	Systemic arterial compliance	2.40	0.989
C_{Ba} [ml/mmHg]	Cerebral arterial compliance	0.358	3.18
M_{CO_2} [ml_{stpd}/s]	Body CO_2 tissue metabolism	4.22	4.89
M_{B,CO_2} [ml_{stpd}/s]	Brain CO_2 tissue metabolism	1.04	1.24
V_{Btis,O_2} [ml_{stpd}]	Cerebral tissue CO_2 volume	900	855
V_D [ml_{btps}]	Total dead space volume	181	201

Table 2

Typical (from literature) state changes in CHF for patient with an enlarged left ventricle.

State	Value	Source
Mean p_{Pa} [mmHg]	increase	[51]
Mean p_{Pv} [mmHg]	increase	[52, 53]
Mean p_{Sa} [mmHg]	decrease or stable	[54]
Mean p_{Sv} [mmHg]	increase	[53]
Mean p_{lv} [mmHg]	steady to increase	[55]
Mean p_{la} [mmHg]	increase	[54]
Left ventricular end-diastolic pressure [mmHg]	increase	[55]
Left ventricular end-systolic pressure [mmHg]	steady or increase	[55]
Left ventricular end-diastolic volume [ml]	increase	[56, 54]
Left ventricular end-systolic volume [ml]	increase	[56, 54]
Left ventricular EF [ml]	decrease	[56, 57]
CO [mlmin]	decrease	[54]
SV [ml]	decrease	[54]
H [beat/min]	increase	[54, 57]
Systemic resistance [mmHg · s /ml]	increase	[53]
Fluid retention [ml]	increase	[53, 58]

Table 3

Nominal parameters and initial conditions for the cardiovascular model. Top: auxiliary parameters, center: model parametersl, bottom: initial values for ODE's.

Parameter	Physiologic description	Nominal value	Reference
EDV_l [ml]	End-diastolic volume (left ventricle)	312	[27]
EDV_r [ml]	End-diastolic volume (right ventricle)	100	[23, 26]
EF	Ejection fraction	0.26	meas
N SV [ml]	Stroke volume	$EF \cdot EDV_l = 81.1$	(19) [23, 26]
ESV_l	End-systolic volume (left ventricle)	$EDV_l - SV = 231$	(19) [23, 26]
ESV_r	End-systolic volume (right ventricle)	$EDV_r - SV = 18.9$	(19) [23, 26]
$\bar{H}$ [bpm]	Mean heart rate	mean (H^d) = 62.5	meas
CO [l/min]	Cardiac output	$SV \cdot \bar{H} = 5.07$	(21) [23, 26]
$p_{l,sys}$ [mmHg]	Systemic left ventricular pressure	$\max\left(p_{sa}^d\right) = 120$	meas
$p_{r,sys}$ [mmHg]	Systemic right ventricular pressure	30	[23, 26]
$p_{l,dia}$ [mmHfg]	Diastolic left ventricular pressure	3	[23, 26]
$p_{r,dia}$ [mmHg]	Diastolic right ventricular pressure	6	[23, 26]
$\bar{p_{Pa}}$ [mmHg]	Mean pulmonary arterial pressure	20	[23, 26]
$\bar{p_{Pv}}$ [mmHg]	Mean pulmonary venous pressure	3.3	[23, 26]
$\bar{p_{Sa}}$ [mmHg]	Mean systemic arterial pressure	$\text{mean}\left(p_{Sa}^d\right) = 79.5$	meas
$\bar{p_{Sv}}$ [mmHg]	Mean systemic venous pressure	6.6	[23, 26]
$\bar{p_{Ba}}$ [mmHg]	Mean cerebral arterial pressure	$0.99\ \bar{p_{sa}} = 78.7$	meas
$\bar{p_{Bv}}$ [mmHg]	Mean cerebral venous pressure	7	[23, 26]
$\bar{qS}$ [ml/s]	Mean systemic flow	0.8 CO = 67.6	[23, 26]
$\bar{q_{Ba}}$, $\bar{q_B}$, $\bar{q_{Bv}}$ [ml/s]	Mean cerebral flow	0.2 CO = 16.6	[23, 26]
$\bar{q_{Pa}}$, $\bar{q_P}$, $\bar{q_{Pv}}$ [ml/s]	Mean pulm flow	CO = 84.5	[23, 26]
V_t [ml]	Total blood volume	5,408	(20) [32]
$\bar{V_{Sa}}$ [ml]	Mean systemic arterial blood volume	$0.1178\ V_t = 637$	[32]
$\bar{V_{Sv}}$ [ml]	Mean systemic venous blood volume	$0.6091\ V_t = 3294$	[32]
$\bar{V_{Ba}}$ [ml]	Mean cerebral arterial blood volume	$0.0237\ V_t = 128$	[32]
$\bar{V_{Bv}}$ [ml]	Mean cerebral venous blood volume	$0.0936\ V_t = 521$	[32]
$\bar{V_{Pa}}$ [ml]	Mean pulmonary arterial blood volume	$0.0288\ V_t = 156$	[32]
$\bar{V_{Pv}}$ [ml]	Mean pulmonary venous blood volume	$0.1243\ V_t = 1672$	[32]
$T_{M,f}$	Time to end-systole	0.35	[29]
$T_{R,f}$	Ventricular relaxation time	$T_{M,f}/2 = 0.175$	[29]
V_{dl} [ml]	Zero left ventricular end-diastolic volume	90	[27]
V_{dr} [ml]	Zero right ventricular end-diastolic volume	10	[12]
$E_{D,l}$ [mmHg/ml]	Left ventricular diastolic elastance	$p_{l,dia}/(EDV_l - V_{dl}) = 0.0135$	(18)

Parameter	Physiologic description	Nominal value	Reference
$E_{D,r}$ [mmHg/ml]	Right ventricular diastolic elastance	$p_{r,dia}/(\mathrm{EDV}_r - V_{dr}) = 0.0667$	(18)
$E_{S,l}$ [mmHg/ml]	Left ventricular systemic elastance	$p_{l,sys}/(\mathrm{ESV}_l - V_{dl}) = 0.849$	(18)
$E_{S,r}$ [mmHg/ml]	Right ventricular systemic elastance	$p_{r,sys}/(\mathrm{ESV}_r - V_{dl}) = 3.38$	(18)
$R_{i,o}$ [mmHg s/ml]	Open $i = mv, ao, tv, pv$ valve resistance	0.001	est
$R_{i,c}$ [mmHg s/ml]	Closed $i = mv, ao, tv, pv$ valve resistance	20	est
R_S [mmHg s/ml]	Systemic resistance	$(\bar{p_{Sa}} - \bar{p_{Sv}})/\bar{q_S} = 1.08$	(22)
R_B [mmHg s/ml]	Cerebral resistance	$(\bar{p_{Ba}} - \bar{p_{Bv}})/\bar{q_B} = 4.25$	(22)
R_{Ba} [mmHg s/ml]	Cerebral arterial resistance	$(\bar{p_{Sa}} - \bar{p_{Ba}})/\bar{q_{Ba}} = 0.0471$	(22)
R_{Bv} [mmHg s/ml]	Cerebral venous resistance	$(\bar{p_{Bv}} - \bar{p_{Sv}})/\bar{q_{Bv}} = 0.0237$	(22)
R_P [mmHg s/ml]	Pulmonary resistance	$(\bar{p_{Pa}} - \bar{p_{Pv}})/\bar{q_P} = 0.198$	(22)
C_{Sa} [ml/mmHg]	Systemic arterial compliance	$0.3\ \bar{V_{Sa}}/\bar{p_{Sa}} = 2.40$	(22) [32]
C_{Sv} [ml/mmHg]	Systemic venous compliance	$0.08\ \bar{V_{Sv}}/\bar{p_{Sv}} = 39.9$	(22) [32]
C_{Ba} [ml/mmHg]	Cerebral arterial compliance	$0.22\ \bar{V_{Ba}}/\bar{p_{Ba}} = 0.359$	(22) [32]
C_{Bv} [ml/mmHg]	Cerebral venous compliance	$0.08\ \bar{V_{Bv}}/\bar{p_{Bv}} = 5.95$	(22) [32]
C_{Pa} [ml/mmHg]	Pulmonary arterial compliance	$0.58\ \bar{V_{Pa}}/\bar{p_{Pa}} = 4.52$	(22) [32]
C_{Pv} [ml/mmHg]	Pulmonary venous compliance	$0.11\ \bar{V_{Pv}}/\bar{p_{Pv}} = 22.4$	(22) [32]
κ [cm^2]	Brain-cerebral flow scaling	0.3	est
p_{Pa}^I [mmHg]	Initial pulmonary arterial pressure	20	[23, 26]
p_{Pv}^I [mmHg]	Initial pulmonary venous pressure	3.3	[23, 26]
p_{Sv}^I [mmHg]	Initial systemic arterial pressure	$\mathrm{mean}\left(p_{Sa}^d\right) = 79.5$	meas
p_{Ba}^I [mmHg]	Initial systemic venous pressure	6.6	[23, 26]
p_{Bv}^I [mmHg]	Initial cerebral arterial pressure	$0.99\ p_{sa}^I = 78.7$	meas
p_{Bv}^I [mmHg]	Initial cerebral venous pressure	7	[23, 26]
V_{lv}^I [ml]	Initial left ventricular volume	$\mathrm{EDV}_l = 312$	[27]
V_{rv}^I [ml]	Initial right ventricular volume	$\mathrm{EDV}_r = 100$	[23, 26]

Table 4

Nominal parameters and initial conditions for the respiratory model. Top: auxiliary parameters, center: model parameters, bottom: initial values for ODE's.

Parameter	Physiologic description	Nominal value or formula	Reference
w [kg]	Body weight	83.2	meas
M_{CO_2} [ml_{stpd}/s]	Body CO_2 tissue metabolism	0.85 M_{O_2} = 4.42	[1, 36, 37]
M_{O_2} [ml_{stpd}/s]	Body O_2 tissue metabolism	5.2	[1, 36, 37]
V_{CO_2} [ml_{stpd}]	Body CO_2 tissue volume	15,000	[1, 36, 37]
V_{O_2} [ml_{stpd}]	Body CO_2 tissue volume	6,000	[1, 36, 37]
M_{B,CO_2} [ml_{stpd}/s]	Brain CO_2 tissue metabolism	0.2 M_{O_2} = 1.04	[1, 36, 37]
M_{B,O_2} [ml_{stpd}/s]	Brain O_2 tissue metabolism	M_{B,CO_2} = 1.04	[1, 36, 37]
M_{S,CO_2} [ml_{stpd}/s]	Systemic CO_2 tissue metabolism	$M_{CO_2} - M_B$, CO_2 = 3.38	[1, 36, 37]
M_S, O_2 [ml_{stpd}/s]	Systemic O_2 tissue metabolism	$M_{O_2} - M_B$, O_2 = 4.16	[1, 36, 37]
$V_{Btis,\,CO_2}$ [ml_{stpd}]	Cerebral tissue CO_2 volume	900	[1, 36, 37]
V_{Btis,O_2} [ml_{stpd}]	Cerebral tissue O_2 volume	1,000	[1, 36, 37]
V_{Stis,CO_2} [ml_{stpd}]	Systemic tissue CO_2 volume	$V_{CO_2} - V_{Btis,CO_2}$ = 14,100	[1, 36, 37]
V_{Stis,O_2} [ml_{stpd}]	Systemic tissue O_2 volume	$V_{O_2} - V_{Btis,CO_2}$ = 5,000	[1, 36, 37]
V_{Bcap,CO_2} [ml_{stpd}]	Cerebral capillary CO_2 volume	$f_{V,cap}$ V_{Btis,CO_2} = 9	[21]
V_{Scap,CO_2} [ml_{stpd}]	Systemic capillary CO_2 volume	$f_{V,cap}$ V_{Stis,CO_2} = 141	est [21]
V_{Bcap,O_2} [ml_{stpd}]	Cerebral capillary O_2 volume	$f_{V,cap}$ V_{Btis,O_2} = 10	[21]
V_{Scap,O_2} [ml_{stpd}]	Systemic capillary O_2 volume	$f_{V,cap}$ V_{Stis,O_2} = 50	est [21]
V_D [ml_{btps}]	Total dead space volume	181	[38, 36, 37]
K_{O_2} [ml_{stpd}/ml]	O_2 dissociation coefficient	0.200	[1, 36, 37]
k_{O_2} [$mmHg^{-1}$]	O_2 dissociation coefficient	0.046	[1, 36, 37]
K_{CO_2} [ml_{stpd} /mmHg/ml]	CO_2 dissociation coefficient	0.0065	[1, 36, 37]
k_{CO_2} [ml_{stpd}/ml]	CO_2 dissociation coefficient	0.244	[1, 36, 37]
$K_{O_2}^{\sim}$ [ml_{stpd} /mmHg/ml]	O_2 linearized dissociation coefficient	0.0025	[1, 36, 37]
D_{T,CO_2} [ml/s]	CO_2 diffusion coefficient	9/60 w/K_{CO_2} = 1899	[21]
D_{T,O_2} [ml/s]	O_2 diffusion coefficient	9/60 $w/K_{O_2}^{\sim}$ = 4938	[21]
$f_{V,cap}$ [N.D.]	Tissue-capillary volume fraction	0.01	[21]
p_{D1,CO_2}^{I} [mmHg]	Initial CO_2 partial pressure dead space 1	5	[37, 38]
p_{D1,O_2}^{I} [mmHg]	Initial O_2 partial pressure dead space 1	159	[37, 38]
p_{D2,CO_2}^{I} [mmHg]	Initial CO_2 partial pressure dead space 2	6	[37, 38]

Parameter	Physiologic description	Nominal value or formula	Reference
p^I_{D2,O_2} [mmHg]	Initial O_2 partial pressure dead space 2	158	[37, 38]
p^I_{D3,CO_2} [mmHg]	Initial CO_2 partial pressure dead space 3	7	[37, 38]
p^I_{D3,O_2} [mmHg]	Initial O_2 partial pressure sdead space 3	157	[37, 38]
p^I_{a,CO_2} [mmHg]	Initial systemic arterial CO_2 partial pressure	40	[39]
p^I_{a,O_2} [mmHg]	Initial systemic arterial O_2 partial pressure	100	[40]
c^I_{Stis,CO_2} [ml_{stpd}/ml]	Initial systemic tissue CO_2 concentration	0.543	[40]
c^I_{Stis,O_2} [ml_{stpd}/ml]	Initial systemic tissue MO_2 concentration	0.128	[40]
c^I_{Btis,CO_2} [ml_{stpd}/ml]	Initial brain tissue CO_2 concentration	0.569	[37, 38]
c^I_{Btis,O_2} [ml_{stpd}/ml]	Initial brain tissue O_2 concentration	0.112	[37, 38]
c^I_{Scap,CO_2} [ml_{stpd}/ml]	Initial systemic capillary CO_2 concentration	$c_{Stis,CO_2} - M_S,CO_2 / D_T,CO_2 = 0.541$	(23)
c^I_{Scap,O_2} [ml_{stpd}/ml]	Initial systemic capillary O_2 concentration	$c_{Stis,O_2} - M_S,O_2 / D_T,O_2 = 0.127$	(23)
c^I_{Bcap,CO_2} [ml_{stpd}/ml]	Initial cerebral capillary CO_2 concentration	$c_{Btis,CO_2} - M_B,CO_2 / D_T,CO_2 = 0.568$	(23)
c^I_{Bcap,O_2} [ml_{stpd}/ml]	Initial cerebral capillary O_2 concentration	$c_{Btis,O_2} - M_B,O_2 / D_T,O_2 = 0.111$	(23)